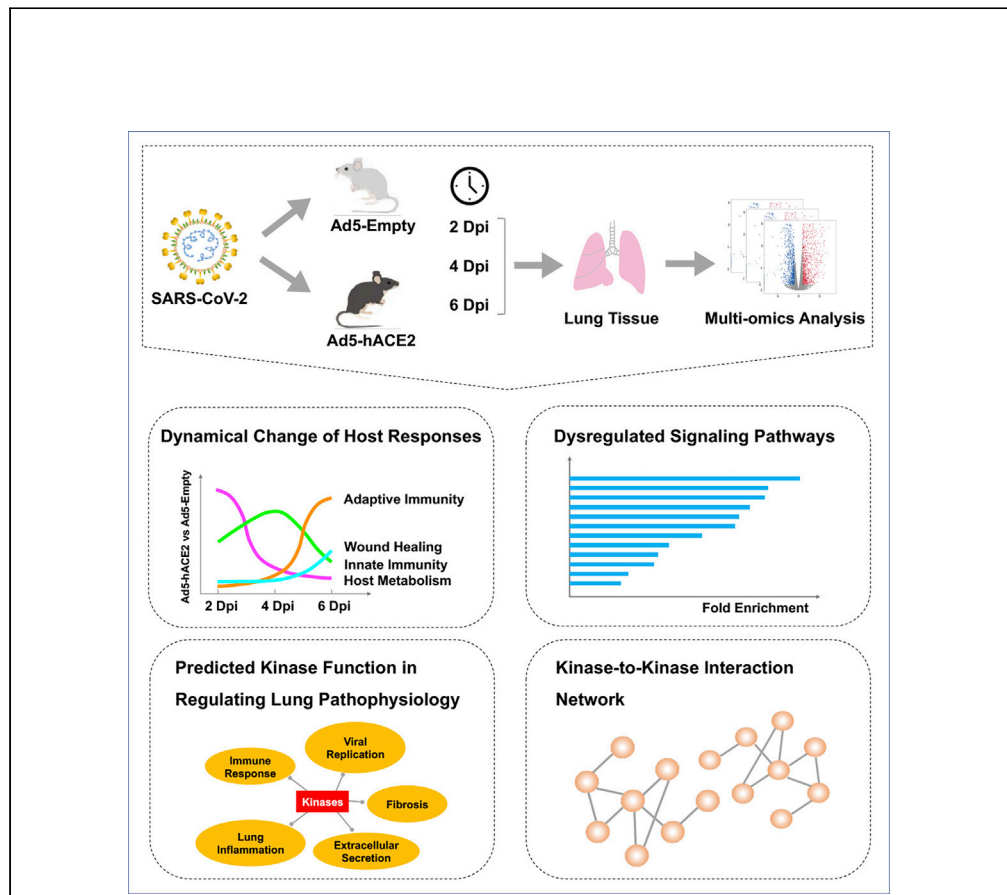


Article

Multi-omics evaluation of SARS-CoV-2 infected mouse lungs reveals dynamics of host responses



Zhao Ni Wang,
Xiang Sheng
Yang, Jing Sun, Jin
Cun Zhao, Nan
Shan Zhong, Xiao
Xiao Tang

tangxiaoxiao@gird.cn

Highlights

Multi-omics analysis profiles temporal host responses in SARS-CoV-2 infected lungs

Signaling pathways and kinase regulating networks are dynamically altered

The CDK and MAPK family are interactive and involved in regulating host responses

Wang et al., iScience 25, 103967
March 18, 2022 © 2022 The Author(s).
<https://doi.org/10.1016/j.isci.2022.103967>



Article

Multi-omics evaluation of SARS-CoV-2 infected mouse lungs reveals dynamics of host responses

Zhao Ni Wang,^{1,3} Xiang Sheng Yang,^{1,3} Jing Sun,^{1,3} Jin Cun Zhao,^{1,2} Nan Shan Zhong,^{1,2} and Xiao Xiao Tang^{1,2,4,*}

SUMMARY

The outbreak of Coronavirus disease 2019 (COVID-19) throughout the world has caused millions of death, while the dynamics of host responses and the underlying regulation mechanisms during SARS-CoV-2 infection are not well depicted. Lung tissues from a mouse model sensitized to SARS-CoV-2 infection were serially collected at different time points for evaluation of transcriptome, proteome, and phosphoproteome. We showed the ebb and flow of several host responses in the lung across the viral infection. The signaling pathways and kinases regulating networks were alternated at different phases of infection. This multiplex evaluation also revealed that many kinases of the CDK and MAPK family were interactive and served as functional hubs in mediating the signal transduction during SARS-CoV-2 infection. Our study not only revealed the dynamics of lung pathophysiology and their underlying molecular mechanisms during SARS-CoV-2 infection, but also highlighted some molecules and signaling pathways that might guide future investigations on COVID-19 therapies.

INTRODUCTION

Coronavirus disease 2019 (COVID-19), caused by a highly transmissible pathogen, severe acute respiratory syndrome coronavirus 2 (SARS-CoV-2), emerged at 2019 and spread rapidly worldwide, exerting a disastrous effect on global health and economy. Within the short twenty years of the 21st century, there have been three strains of highly virulent β coronavirus causing the outbreaks of acute respiratory syndrome, including SARS-CoV in 2002 (Zhong et al., 2003), Middle East Respiratory Syndrome (MERS)-CoV in 2012 (Zaki et al., 2012) and SARS-CoV-2 in late 2019. Compared with the SARS-CoV, SARS-CoV-2 has 10- to 20-fold higher affinity to the host viral receptors (Hoffmann et al., 2020), partially explaining its greater transmission and faster spread. Although currently many clinical trials for candidate drugs and vaccination against SARS-CoV-2 are under way, the pandemic is still ongoing. In addition, considering that there have been three outbreaks of virulent coronavirus within twenty years, it is highly suspected that a new coronavirus would strike again. Therefore, understanding the mechanisms underlying the pathophysiology of COVID-19 is imperative and may also prepare us for the next pandemic.

Lungs are the primary target organs for the SARS-CoV-2 infection. Some autopsy examinations have revealed pathological changes in the lungs of patients who died of COVID-19 (Carsana et al., 2020; Tian et al., 2020; Hooper et al., 2021; Borczuk et al., 2020). Among these changes, mucus hypersecretion and pulmonary fibrosis have caught our attention because they are highly associated with the exacerbation or even demise of infected patients and may also affect the health of survivors. A single cell sequencing analysis of bronchoalveolar lavage fluid (BALF) cells from COVID-19 patients revealed over-expression of gel-forming mucins MUC5AC and MUC5B as well as impairment of mucociliary clearance (MCC) (He et al., 2020), which promoted the mucus plugs formation and airflow limitation. The excessive production of MUC5B was also thought to be an indicator of lung fibrosis (Leng et al., 2020; Wu et al., 2020). The relationship between MUC5B and idiopathic pulmonary fibrosis has been well-depicted (Noth et al., 2013; Hancock et al., 2018; Peng et al., 2022). Proteomics of lung tissues from postmortem COVID-19 patients showed significant dysregulation of the extracellular matrix organization, which is relevant to the pathogenesis of emphysema and lung fibrosis (Leng et al., 2020; Wu et al., 2020). Likewise, Nie et al. found that the majority of the fibrosis-related proteins with differential expression got involved in the modification stage of organism fibrosis, reflecting remodeling of the lung structure in patients with severe COVID-19 (Nie et al., 2021).

¹State Key Laboratory of Respiratory Disease, National Clinical Research Center for Respiratory Disease, National Center for Respiratory Medicine, Guangzhou Institute of Respiratory Health, The First Affiliated Hospital of Guangzhou Medical University, Guangzhou, P. R. China

²Guangzhou Laboratory, Bioisland, Guangzhou, Guangdong, P. R. China

³These authors contributed equally

⁴Lead contact

*Correspondence:

tangxiaoxiao@gird.cn

<https://doi.org/10.1016/j.isci.2022.103967>



However, most previous studies only investigated the lung pathophysiology of severe or decedent COVID-19 patients, while little is known about the dynamics of biological perturbation during the SARS-CoV-2 infection. For ethical reasons, human lung tissue is difficult to obtain from patients of different infection stages. Previous studies merely focused on the epithelial cells or immune cells from BALF or peripheral blood of COVID-19 patients, or lung tissues from COVID-19 decedents who might die of other severe complications. In addition, the vast majority of lung tissues used in omics studies were not freshly harvested or even fixed in formaldehyde solution. These may make the results defective. In addition, the information from these samples is also limited to the endpoint of the disease course, while the early change of lung pathophysiology is scarce.

In these respects, animal models of infection are appropriate alternatives of human lung tissues on investigating the dynamics of COVID-19 pathophysiology and the underlying regulation mechanisms. Previously, we have successfully established a mouse model sensitized to SARS-CoV-2 infection (Sun et al., 2020). By transducing adenoviral vector (Ad5) expressing human angiotensin converting enzyme 2 (hACE2), SARS-CoV-2 could invade and replicate in mouse lungs, causing acute lung injury (ALI) with severe changes at 5 days post infection (dpi), which largely mimicked the COVID-19 lung pathology. By using this model, we performed a multi-omics analysis on lung tissues of different phases of infection (2, 4 and 6 dpi), profiled the molecular changes and pathway dysregulation during the viral infection, and revealed underlying mechanisms of the COVID-19 pathogenesis, with an emphasis on the immunity, pulmonary fibrosis, and airway mucus hypersecretion.

RESULTS

Multiplexed quantitative analysis identified dysregulated genes/proteins/phosphopeptides in mouse lungs during SARS-CoV-2 infection

Mice pre-transduced with Ad5-hACE2 (H) or empty vector (E) were infected with human SARS-CoV-2 virus. As shown in Figure 1A, fresh lung tissues were obtained from mice at 2, 4 and 6 dpi, and then processed to RNA and proteins extraction, TMT tag labeling, and omics analysis of transcriptome, proteome and phosphoproteome, followed by the integrated analysis of these three omics data to obtain further information. We chose the time points of 2, 4 and 6 dpi largely based on the previously published study (Sun et al., 2020) in which the same animal model was used. In SARS-CoV-2 infected Ad5-hACE2 transduced BALB/c mice, the viral load peaked at 1-2 dpi, while it declined to the lowest titer after 6 dpi. At 2 dpi, infected mice started to present symptoms such as ruffled fur, hunching, and difficulty breathing, while body weight loss and pathological changes in lung tissue were the most severe at 6 dpi. Therefore, we consider that 2, 4 and 6 dpi represent the early, middle, and late stage of infection, respectively. The expression value baselines of transcriptome and proteome were previously corrected by using edgeR and Maxquant 1.5.2.8, respectively. By using the criterion of adjusted p value <0.05 and $|\log_2(\text{FC})| > 1$, we identified genes with differential expression (DE) at each time point (Figure 1B) and the entity was considered differentially expressed at even one time point. Through the same way, we also confirmed the DE proteins and DE phosphorylated peptides (Figure 1B). By using heatmaps, we further displayed the dynamical changes of the identified DE genes, proteins, and phosphorylated sites, respectively. Also, we found that most of their expression changed over time (Figure 1C).

SARS-CoV-2 infection reprograms transcriptome in mouse lung

To determine the dynamics of transcriptome in mouse lungs during SARS-CoV-2 infection, we performed a step-by-step computational analysis from co-expression clustering analysis to protein-protein interaction (PPI) networking (Figure 2A). First, based on strict criteria, we identified 1,626 genes with differential expression between H and E groups at any time point. Among these DE genes, we identified six functional transcriptome clusters (TC) associated with SARS-CoV-2 infection through Mfuzz expression pattern clustering analysis (Kumar and Futschik, 2007) (Figure 2B). The conventional hard clustering of data wherein one gene is assigned to one exact cluster may lead to information loss. In contrast, soft clustering can overcome this shortcoming by assigning one gene to several clusters. Mfuzz analysis, a soft clustering technique implemented using the fuzzy c-means algorithm, is based on the iterative optimization of an objective function to minimize the variation of objects within clusters. Poorly clustered objects reduce influence on the resulting clusters and make the clustering process less sensitive to noise. The membership value of one DE gene produced by Mfuzz analysis indicates the degree of membership of this gene in the related cluster. The genes in each cluster shared similar regulation mechanisms. TC4 presented a progressive decline in overall signals over time while TC1 showed an increase in gene expression. Through KEGG analysis

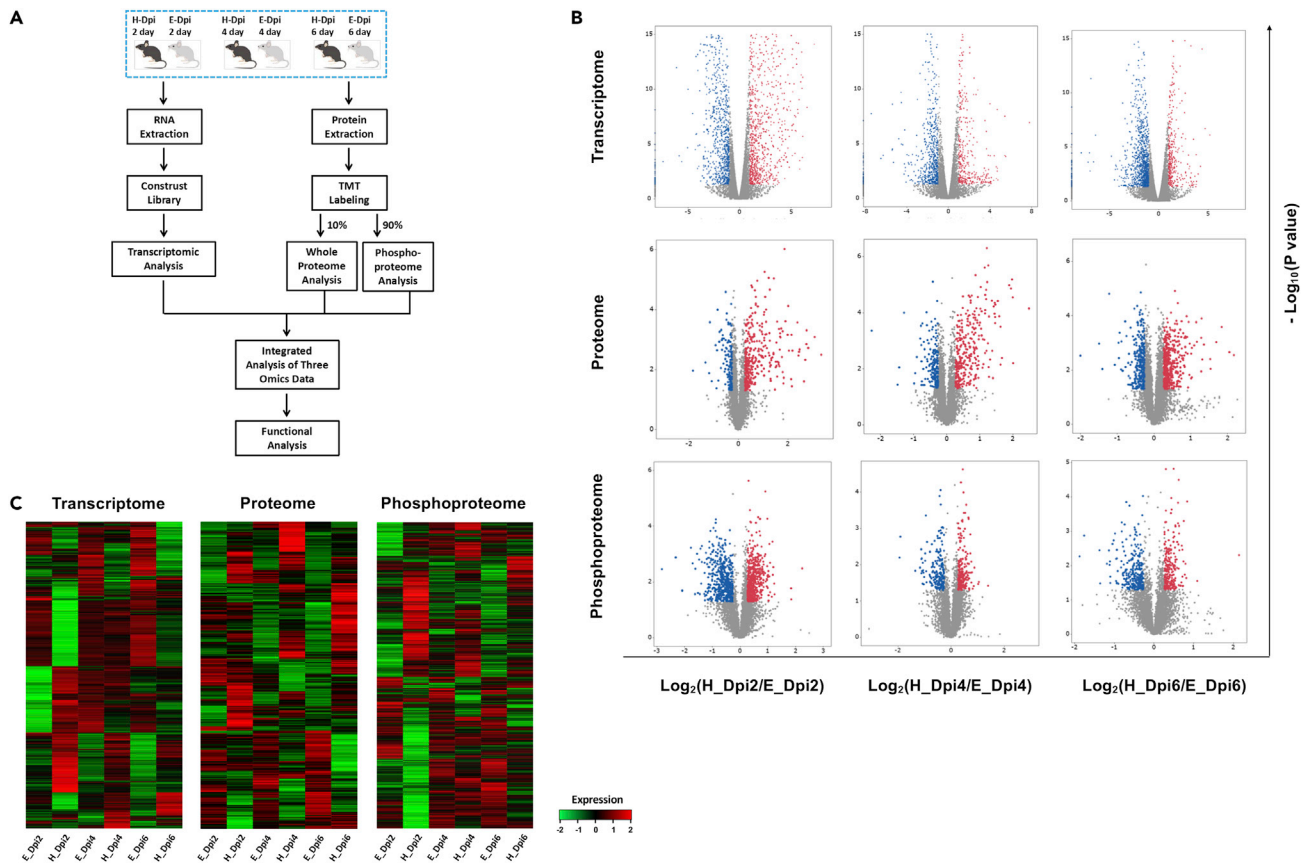


Figure 1. Profiling of transcriptome, proteome and phosphoproteome during SARS-CoV-2 infection in mice

(A) Experimental scheme for transcriptome, proteome and phosphoproteome measurement. SARS-CoV-2 was administrated intranasally into mice pre-transduced with Ad5-hACE2 (H) or empty vector (E). All conditions were performed in biological triplicates.

(B) Volcano plots of the transcripts, protein abundance and phosphorylation sites. Dysregulated genes, proteins and phosphorylation sites outside the significance threshold lines were colored in blue (downregulated) or red (upregulated).

(C) Heatmap of dysregulated genes, proteins and phosphorylation sites were shown.

The cutoff of dysregulation was set at adjusted p value < 0.05 and $|\log_2(FC)| > 1$ for genes, and adjusted p value < 0.05 and $|\log_2(FC)| > \log_2(1.2)$ for proteins and phosphorylation sites.

(Figure 2C), we found that TC2 was enriched DE genes associated with the activation of oxytocin signaling and adrenergic signaling, cardiac or vascular smooth muscle contraction, and gastric acid secretion, reflecting the strong neurohumoral stress response at an early phase of infection. As shown in TC4, metabolic pathways and the innate immune responses like IgA production were also rapidly induced at 2 dpi and then gradually simmered down. On the contrary, pathways enriched in TC1 were increasingly activated during the viral infection, regarding cell proliferation (e.g., cell cycle, DNA replication) and adaptive immunology (e.g., T-cell receptor signaling pathway). TC6 showed a rapid increase at 4 dpi and was associated with thrombogenesis (e.g., complement and coagulation cascade, platelet activation) and glycoprotein production (e.g., N-Glycan biosynthesis).

To further determine the function and regulation of the genes in each cluster, we performed a PPI network modulization with the corresponding proteins of DE genes. We identified 13 PPI modules and determined their functions based on known database like GO and KEGG (Figure 2D). Module 2 included DE genes correlating to viral protein interaction with cytokines and cytokine receptors. Module 3 showed the defense response to virus and Module 13 reflected the neutrophil degranulation upon SARS-CoV-2 infection. These interactive modules showed the activation of innate immune response against SARS-CoV-2 infection. Genes in Module 4 were correlated to muscle contraction and platelet activation. Modules 5 and 7 included DE genes associated with cornified envelope formation, and Module 1 contained cell cycle related genes, probably indicating the regeneration of lung structure cells and the expansion of immune cells in mouse

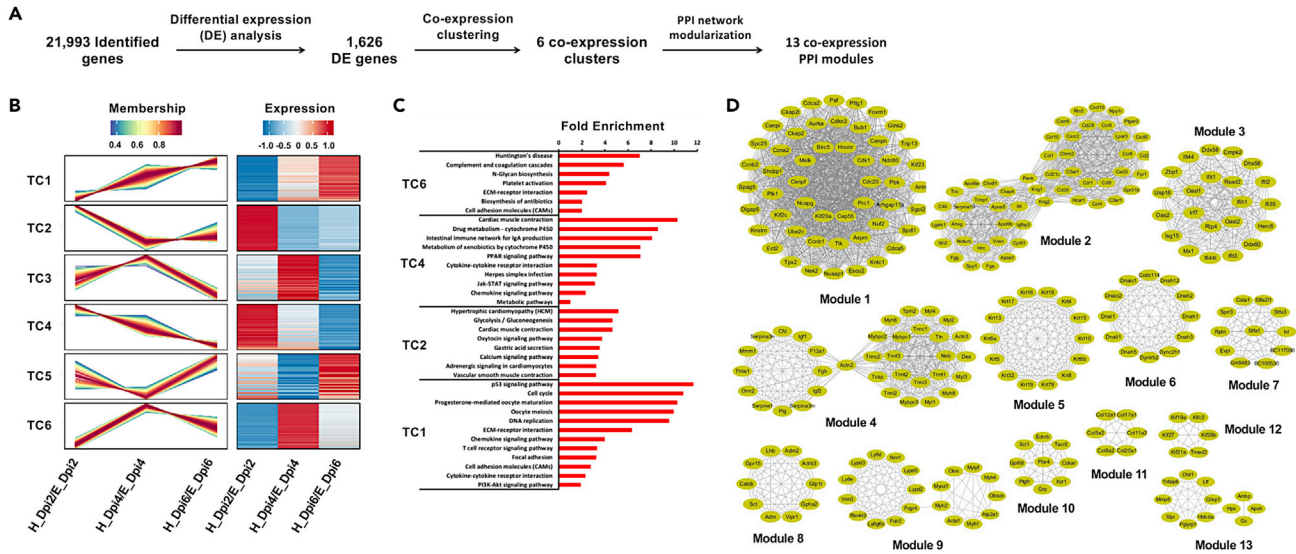


Figure 2. Transcriptional expression profile revealed co-expression clusters and functional modules during SARS-CoV-2 infection in Ad5-hAEC2 mice

(A) Flow chart of transcriptome analysis.

(B) Clusters of DE genes in lung tissues of SARS-CoV-2 infected mice versus mock controls. Each graph at the left side was composed of a bunch of membership lines and each line represented one DE gene. The color of the line indicates the membership degree. The darker the red is, the higher the membership degree is. The y axis indicated the relative gene expression. The heatmap at the right side showed the relative gene expression.

(C) Pathway enrichment and functional annotation of DE genes in TC1, TC2, TC4 and TC6 by KEGG.

(D) Thirteen interconnected modules derived from DE genes. The gene names are shown in the circle.

TC, transcriptome cluster

lungs. Six collagen genes in Module 11 were associated with extracellular matrix organization reflecting the lung structure remodeling. Modules 2, 9 and 12 reflected the activation of protein translation, modification, and trafficking.

Proteomic perturbation in mouse lungs upon SARS-CoV-2 infection

By using the similar stepwise computational analysis (Figure 3A), we sought to profile the proteomic perturbation in lung tissues from SARS-CoV-2 infected mice. 1,199 DE proteins were identified from the whole 6,917 proteins, and then were clustered into six proteome clusters (PC) according to their expression patterns across the viral infection through Mfuzz analysis (Figure 3B). Proteins in PC1 and PC5 showed a gradual decline in the protein abundance during infection, while those in PC3 and PC4 present an increasing pattern. By further analyzing the DE proteins in these clusters by KEGG pathway enrichment (Figure 3C), we found that PC5 was rich in metabolism pathways, indicating that cell metabolism was rapidly triggered upon viral infection and then downregulated. Similarly, proteins in PC1 showed the enrichment of pathways correlated to cytokine and chemokine production (e.g., chemokine signaling pathway and PI3K-Akt pathway), which were activated at 2 and 4 dpi while downregulated at 6 dpi. These signaling pathways contribute to the rapid innate immune response, while pathways in PC3 and PC4 were later activated and more correlated to the adaptive immune response, such as T and B cell receptor signaling in PC3 and T helper cell (Th1, Th2 and Th17) differentiation in PC4, suggesting the transition of innate to adaptive immune defense at 6 dpi in mouse lungs. Proteins in PC4 were also enriched in other viral infections, indicating that SARS-CoV-2 infection shares some features with other infections. Besides, pathways in PC3 and PC4 also revealed the later induction of cell death (e.g., apoptosis, autophagy) and cell proliferation (e.g., cell cycle, VEGF signaling), showing the synchronization of lung injury and regeneration upon SARS-CoV-2 infection, in accordance to the pathology of lung tissue damage and repair in COVID-19 patients.

We further performed the PPI network modularization among the DE proteins and identified eight co-expressing modules (Figure 3D). PPI 2 was referred to complement and coagulation cascades, consistent with thrombosis found in COVID-19 decedents (Nie et al., 2021). The thrombosis was also attributable

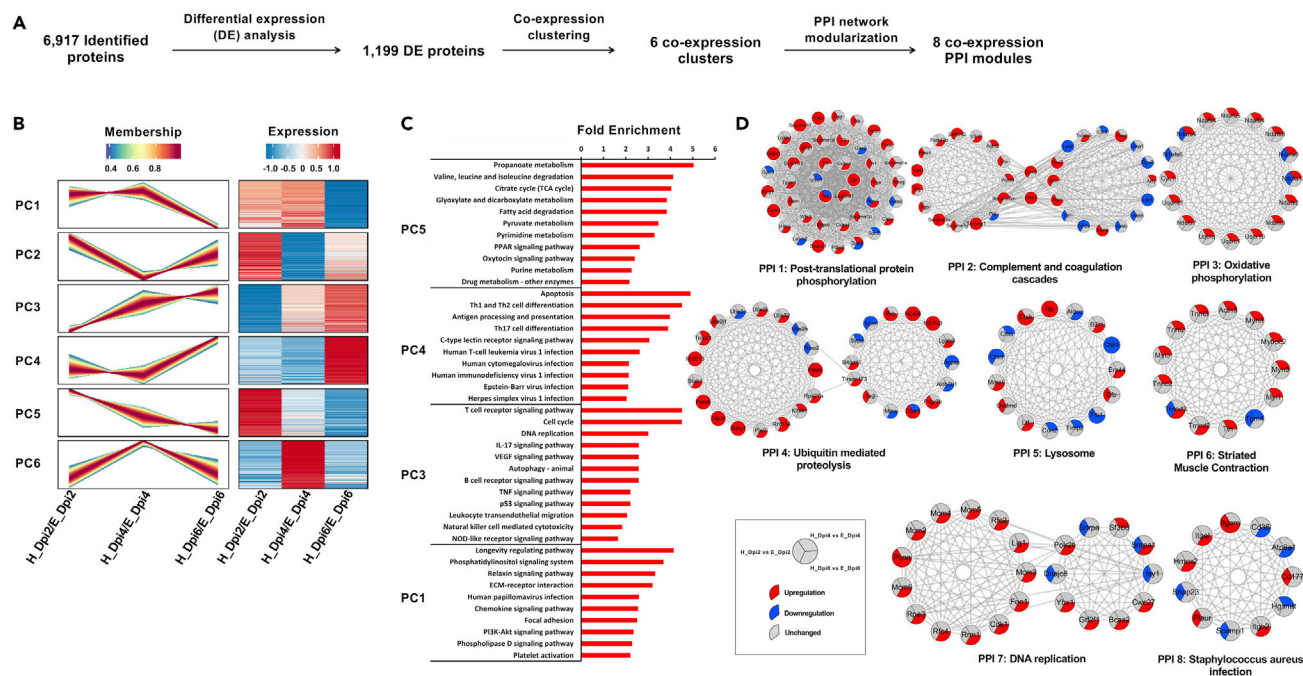


Figure 3. Proteomic perturbation in mouse lungs upon SARS-CoV-2 infection

(A) Flow chart of proteome analysis.

(B) Clusters of DE proteins in lung tissues of SARS-CoV-2 infected mice versus mock controls. Each graph at left was composed of a bunch of membership lines and each line represented one DE protein. The y axis indicated the relative protein abundance. The heatmap at the right side showed the relative protein abundance.

(C) Pathway enrichment and functional annotation of DE proteins in PC1, PC3, PC4 and PC5 by KEGG.

(D) Significantly interaction networks derived from DE proteins.

Each circle represents one protein with its gene name marked inside. Three sectors in one circle represents three time points of infection, and red, blue and gray color indicates increase, decrease and no change in expression, respectively. PC, proteome cluster.

to neutrophil activation (Noubouossie et al., 2019), which was indicated by upregulation of Plaur, Itgb2, Cd177 and Hmox2 in PPI 8. Proteins in PPI 4 and PPI 5 functioned in protein degradation. However, some proteins related to lysosome biogenesis were downregulated during viral infection, such as Ctsd. Lysosome formation is a key step for the complete process of autophagy, which plays an important role in host defense by degrading virus proteins, damaging virus-infected cells and processing antigens (Deric et al., 2013). Recent studies have demonstrated that SARS-CoV-2 viral protein ORF3a could block fusion of autophagosomes/amphisomes and lysosome, thus facilitating viral replication (Miao et al., 2021; Qu et al., 2020; Gassen et al., 2020). In addition, PI3K-Akt pathway activation can reduce autophagy through its downstream factor-mammalian target of rapamycin complex 1 (mTORC1). Thus, upregulation of PI3K pathway at 2 and 4 dpi might have left enough time allowing the viral replication, spreading and evasion from the host immunity (Figures 3B and 3C). Notably, matrix metalloproteinase-9 (Mmp9) in PPI 5 was increased at 6 dpi. Collagenase Mmp9 is upregulated in many chronic diseases including asthma, chronic obstructive pulmonary disease (COPD) and pulmonary fibrosis (Atkinson and Senoir, 2003), getting involved in the extracellular matrix deposition. PPI 1 and PPI 3, in which most proteins were upregulated, were associated with protein phosphorylation, indicating the activation of signaling pathways after SARS-CoV-2 infection.

Based on the highly activated protein phosphorylation (Figure 3D), we further analyzed dysregulated kinases in response to SARS-CoV-2 infection. DE kinases were grouped into six clusters (Figure S1A) according to their expression patterns and biological functions. PKR and MLKL were upregulated at all time points, getting involved in interferon mediated-necroptosis upon viral infection (Balachandran et al., 2000; Sarhan et al., 2019). MAPKAPK2, RIPK3, JAK3 were not apparently intrigued until 6 dpi, and served to regulate lung inflammation through activating MAPK signaling cascade, NF- κ B and JAK-STAT pathway. Pathway analysis of the DE kinases showed significant enrichment in VEGF signaling, chemokine signaling,

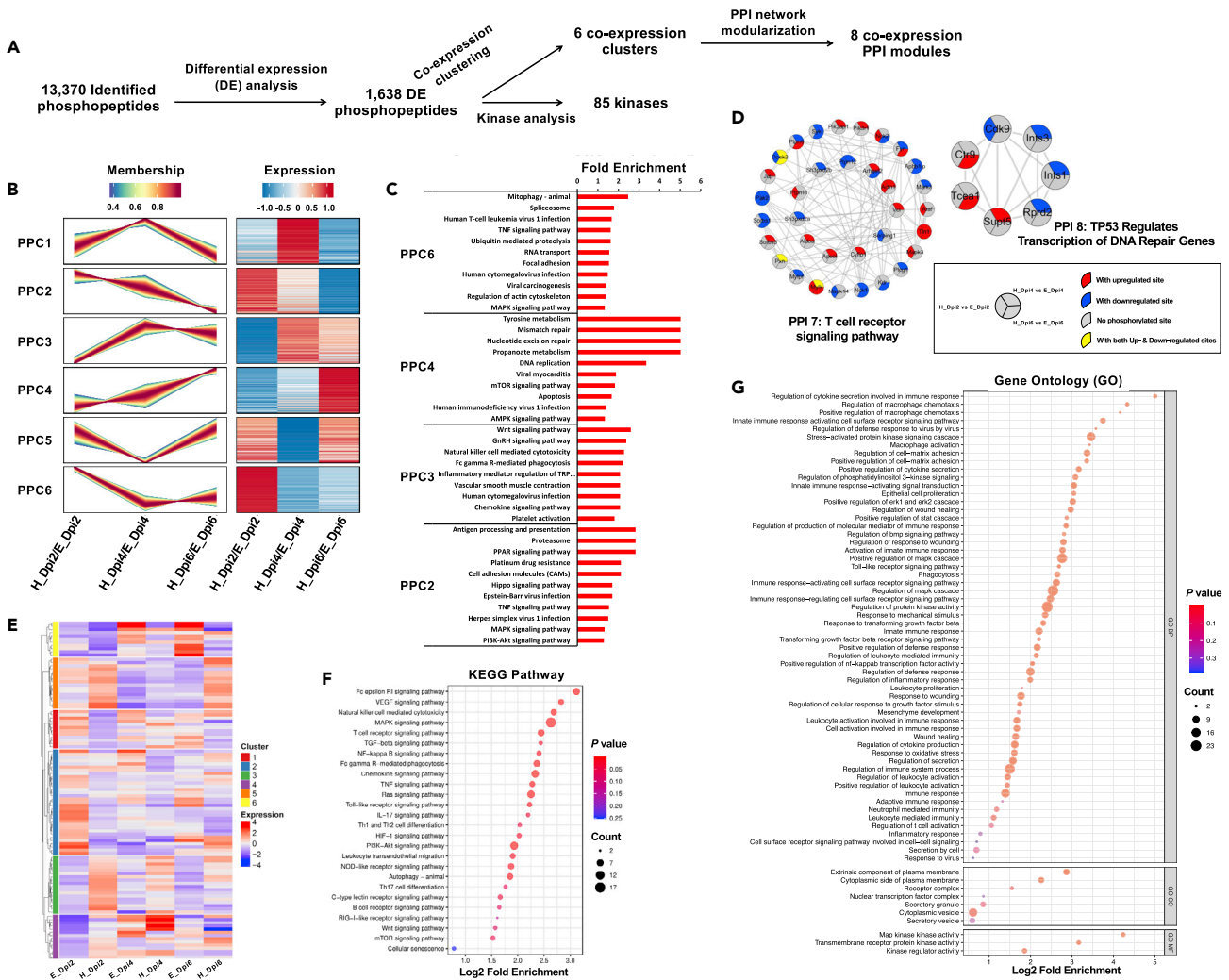


Figure 4. Phosphoproteomic analysis revealed dysregulated pathways and annotated functions of kinases in SARS-CoV-2 infected mouse lung (A) Flow chart of phosphoproteomic analysis.

(B) Clusters of DE phosphopeptides in lung tissue of SARS-CoV-2 infected mice versus mock controls.

(C) KEGG pathway enrichment analysis of dysregulated phosphopeptides in the lung tissues.

(D) Interactive networks of dysregulated phosphopeptides. Each sector represents each time point of infection, with red, blue and gray indicating increased, decreased and unchanged expression, respectively, and yellow indicates that the protein is both modified by upregulated and downregulated phosphorylated sites.

(E) Clusters of kinases with phosphorylation change.

(F) Pathway enrichment of phosphorylated kinases with activity change by KEGG analysis.

(G) Perturbed phosphorylated kinases associated biological process (BP), cellular component (CC) and molecular function (MF) are presented through GO analysis.

PPC, phosphoproteome cluster.

Ras signaling, MAPK signaling, PI3K-Akt signaling, p53 signaling, necroptosis and cellular senescence (Figure S1B). Gene ontology (GO) analysis also indicated their roles in signal transduction, defense response to virus, activation of innate and adaptive immunity and cellular metabolic process (Figure S1C).

Phosphoproteomic analysis revealed dysregulated pathways and annotated functions of kinases in SARS-CoV-2 infected mouse lung

Among 13,370 identified phosphopeptides, we recognized 1,638 dysregulated DE phosphopeptides upon SARS-CoV-2 infection in mouse lung (Figure 4A). Through co-expression clustering, we grouped these DE phosphopeptides into six phosphoproteome clusters (PPC) through Mfuzz clustering analysis (Figure 4B).

We further performed pathway enrichment of PPC2, 3, 4 and 6 (Figure 4C), in which the expression of phosphopeptides were consecutively upregulated (PPC3 and PPC4) or downregulated (PPC2 and PPC6) across the time course of infection. As compared to DE proteins (Figure 3C), some pathways enriched in DE phosphopeptides share the same dynamical patterns, such as rapid activation of focal adhesion, PI3K-Akt pathway and PPAR pathway at the early phase of infection, and later induction of DNA replication, apoptosis and natural killer cell mediated cytotoxicity. However, some pathways were regulated differentially between proteome and phosphoproteome, like chemokine signaling pathway, platelet activation, TNF signaling and antigen processing and presentation, indicating that regulation machineries of protein translation and phosphorylation is not always coordinated. In the phosphoproteome of mouse lungs, we found that MAPK signaling pathway (in PPC2 and PPC6) was predominantly dysregulated, showing a quick response at 2 dpi and subsequent downregulation at 4 and 6 dpi (Figures 4B and 4C), probably accounting for the early innate immune response against the virus (Arthur and Ley, 2013).

The DE phosphopeptides could be clustered into eight protein interaction networks through PPI modulation (Figures 4D and S2). Most of these interaction modules were referred to protein synthesis, transportation, modification and degradation (Figure S2: PPI 1, 3, 4, 5 and 6), reflecting the active biological reactions upon SARS-CoV-2 infection. Some modules were correlated to the T cell receptor signaling pathway (Figure 4D: PPI 7) or p53-regulated DNA Repair (Figure 4D: PPI 8). We also discovered an upregulation of MAPK signaling pathway in PPI 7 (e.g., Mapk3, Araf, Vcl, Tln1), suggesting its potential role in activating T-cells. This implicated that MAPK pathway got involved in regulating both innate and adaptive immunity in the SARS-CoV-2 infected lungs.

To further understand the regulation of signaling pathways during viral infection, we also screened out the phosphorylated kinases from DE phosphopeptides and clustered them into six groups according to their expression profile (Figure 4E). KEGG pathway enrichment revealed several pathways regulated by these kinases, including MAPK signaling, T-cell receptor signaling, TGF- β signaling, chemokine signaling and PI3K-Akt signaling pathway (Figure 4F). GO analysis showed that they were getting involved in protein phosphorylation and signal transduction, such as positive regulation of MAPK signaling pathway, immune response, cell proliferation, wound healing etc (Figure 4G).

Integrative analysis of proteome and phosphoproteome revealed kinase activity and their predicted roles during SARS-CoV-2 infection

As proteome and phosphoproteome have their own unique features, integrative analysis of these two omics data may bring us new perspectives on the lung pathophysiology upon SARS-CoV-2 infection. We analyzed and predicted the interrelationship between the activated kinases and DE phosphorylated sites. The interactive networks present differential regulation patterns of kinases on their underlying substrates at different time points post infection (Figure S3). The number of phosphorylated sites and kinase-to-phosphorylated site connections at 2 dpi was larger than those of the other two time points, indicating that kinases have responded instantly following the SARS-CoV-2 invasion and played a leading role in regulating the host responses against the viral infection. We also found that the hubs of the networks were always of MAPK family (e.g. ERKs, P38D, JNK1) and cyclin-dependent kinases (CDKs) at different time points, reinforcing the importance of these kinases and their downstream signaling pathways in the lung pathogenesis during the SARS-CoV-2 infection (Figure S3).

The type and number of activated kinases also changed during SARS-CoV-2 infection (Figures 5A and S4). According to the kinase activity score, we identified the top 10 positive and negative kinases. CDK family have accounted for most of the positive kinases at 2 dpi. CDKs play key roles in controlling cell expansion as well as gene transcription. The role of CDKs in viral replication has also been demonstrated (Gutierrez-Chamorro et al., 2021): During human immunodeficiency virus (HIV) replication, CDK7 and CDK9 serve as part of the RNA-pol II initiation and elongation complexes; CDK8 promotes the transcription of viral genome, while CDK11 and CDK13 (CHED) contribute to processing the viral transcript. Previous study has reported that CDK2 and CDK4 were upregulated during SARS-CoV-2 infection (Bouhaddou et al., 2020), while we firstly demonstrate that CDK7/8/9/13 were also activated at early stage of SARS-CoV-2 infection when viral replication was highly active. Thus, it is very likely that these CDKs also participate in the SARS-CoV-2 replication cycle. The role of CDKs in inflammation is also of concern. CDK5 has numerous physiological functions (Sharma and Sicinski, 2020), and it is an activator of IFN- γ -activated inhibitor of translation (GAIT) pathway, which facilitated exacerbation of inflammation (Arif et al., 2011). Besides, CDK8 was identified

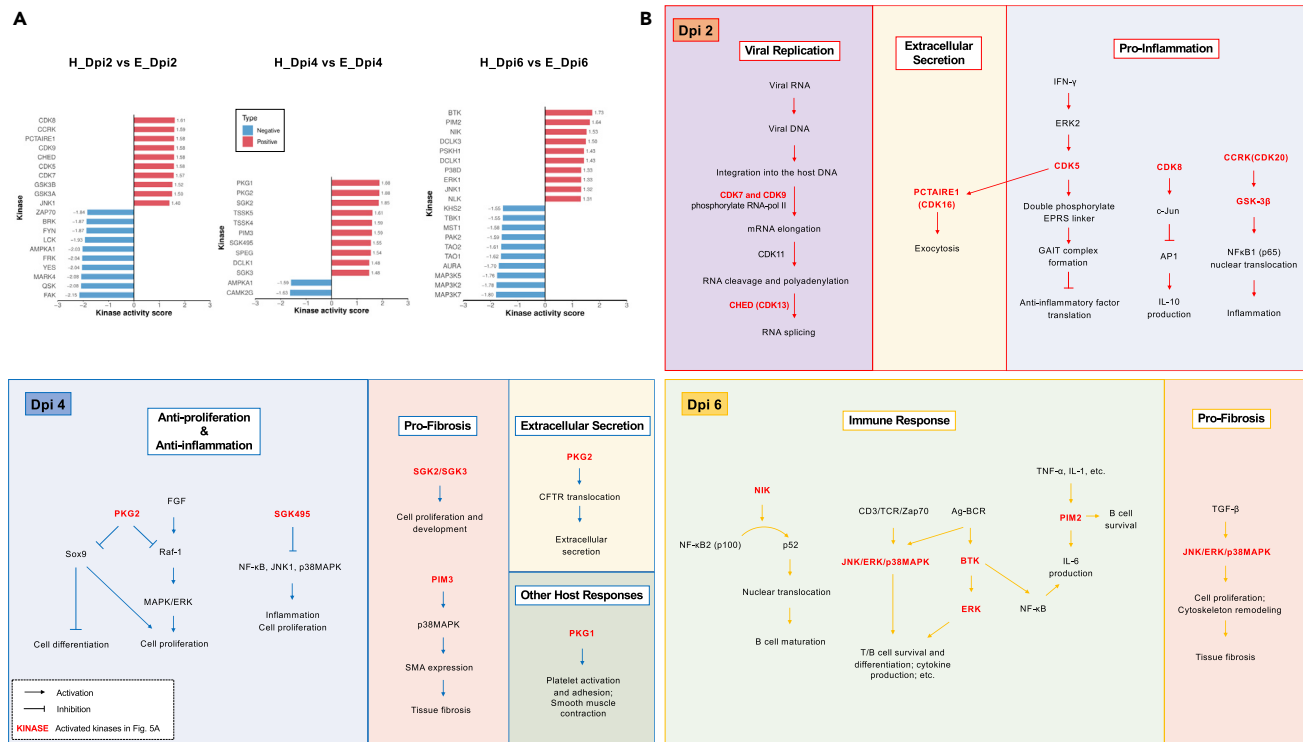


Figure 5. Integrative analysis of proteome and phosphoproteome revealed dynamics of kinase activity and their predicted roles in SARS-CoV-2 infection

(A) Activity score of kinases with significant change in both proteome and phosphoproteome. (B) Schematics of the predicted roles of activated kinases in regulating host responses upon SARS-CoV-2 infection.

as a potential pro-inflammatory factor reducing production of anti-inflammatory cytokine IL-10 during innate immune response (Johannessen et al., 2017).

GSK-3β, a classic component of Wnt signaling, is also highly activated at 2 dpi. GSK-3β also gets involved in the activation of NF-κB pathway by promoting phosphorylation of p65 and its transportation to nuclear, thus mediating the inflammatory response (Hoefflich et al., 2000). In this regard, CCRK (CDK20) was demonstrated as an activator of GSK-3β and mTORC signaling (Sun et al., 2018). These evidences implicated that CDK5, CDK8, CCRK (CDK20) and GSK-3β may be potential targets for anti-inflammation therapy in COVID-19.

At 4 dpi, cGMP-dependent protein kinases (PKGs) and serum- and glucocorticoid-inducible kinases (SGKs) were significantly activated. PKG1/2 are serine/threonine protein kinases activated by cGMP. PKG1 can phosphorylate numerous target proteins, regulating lots of biological processes, such as platelet activation and adhesion and smooth muscle contraction (Hofmann et al., 2006). PKG2 phosphorylation is essential for intestinal secretion by promoting CFTR translocation in jejunum (Golin-Bisello et al., 2005). PKG2 negatively regulates growth factors-mediated ERK/MEK activation and cell proliferation (Kamemura et al., 2017). Wang et al. also discovered that PKG2 inhibited cell proliferation and favored cell differentiation in human and mouse colon cells through reducing Sox9 expression and its mediated signaling (Wang et al., 2012). SGKs work synergistically with Akt to propagate the effects of PI3K activation and mediates cell survival and cell cycle progression (Brunet et al., 2001). Elevation of SGK2/3 is linked to tumor development (Basnet et al., 2018). SGK495/STK40 participates in stem cell development and differentiation. It can negatively regulate the activation of NF-κB, JNK1 and p38MAPK, thus may inhibit inflammation mediated by these signals (Hu et al., 2019; Taccioli et al., 2015; Li et al., 2010). PIM3 may promote lung fibrosis by up-regulating expression of p38 MAPK and smooth muscle actin (SMA) (Yang et al., 2017).

At late phase of infection, activated kinases seemed to regulate the immune response and inflammation. Bruton's tyrosine kinase (BTK) is indispensable for the development and differentiation of B cells (Khan,

2001). It is also required for TLR8/9-mediated NF- κ B activation and IL-6 production during viral infection (Doyle et al., 2007). PIM2 is essential for cell survival and may enhance lipopolysaccharide-induced IL-6 production (Yang et al., 2010). PIM2 is favorable for B cell survival but inhibits T cell-mediated immune response (Liu et al., 2020b). NIK(MAP3K14) is involved in NF- κ B pathway activation by phosphorylating NF- κ B2 (p100), leading to production and nuclear translocation of p52, which is associated with lymphogenesis and B cell maturation (Senftleben et al., 2001). JNK, nemo-like kinase (NLK) and p38 MAPK are known downstream targets for MAP3K7. MAP3K7-NLK signaling negatively regulates the activation of canonical Wnt pathway, which modulates cell migration and adhesion (Katoh and Katoh, 2009). In addition, p38, ERK and JNK are involved in many biological mechanisms, including B and T cell receptor signaling and TGF- β /Smad signaling.

Doublecortin-like kinase 1 (DCLK1) was activated at both 4 and 6 dpi (Figures 5A and S4). It is a marker of turf cells, which are the main source of IL-25 in intestine, thymus and nasal polyps (Gerbe et al., 2016; Miller et al., 2018; Kohanski et al., 2018). However, the role of turf cells in lungs and the COVID-19 disease has not been demonstrated. In this study, we also found that DCLK1 is the upstream of tight junction protein ZO-1 (Figure S3), indicating its potential role in mediating damage of airway epithelium integrity during viral infection, as phosphorylation of ZO-1 could reduce its location at cell junctions (Abdala-Valencia et al., 2018).

Together, we conclude the potential functions of the activated kinases in regulating the host responses at different stages of SARS-CoV-2 infection in lungs (Figure 5B). These kinases mediate numerous biological processes during viral infection, including viral replication, inflammation, immune response, extracellular secretion and lung fibrosis. The regulation machineries existed to be time-varying, and most biological processes mediated by them were coordinated with the COVID-19 pathophysiological changes. For example, CDKs were induced at early phase with functions of regulating DNA replication and inflammation, while PIM3 and PIM2 were activated at a later phase to promote tissue remodeling and B cell-mediated immune response, respectively (Figure 5B). However, the relationship of these kinases and the host responses upon SARS-CoV-2 still needs to be further verified.

Reconstruction of signaling pathways and kinase interaction network by integrative profiling of transcriptome, proteome and phosphoproteome

Through Pearson's correlation analysis (Figure 6A), we found that nearly half of the transcripts were negatively correlated with their corresponding proteins on expression profiles, suggesting the necessity to integrate the transcriptomic and proteomic data. Therefore, we performed Gene Set Enrichment Analysis (GSEA) on the whole transcripts as well as proteins of mouse lung, and reconstructed the signaling networks upon SARS-CoV-2 infection (Figure 6B). Most of the upregulated signaling pathways were correlated to pathogen infections. Next, we screened out transcripts and proteins that were overlapped between Transcriptome and Proteome, and clustered them into 6 modules (Figure 6C). These transcriptome and proteome clusters (TPC) were processed to pathway enrichment through KEGG analysis (Figure 6D). DE proteins and genes in TPC6 were upregulated instantly at 2 dpi and then downregulated. They were enriched in metabolism pathways. TPC2 was also mainly composed of metabolism pathways while they were downregulated during viral infection. Apparently, the metabolism pathways between cluster 2 and 6 were diverse. A recent study has demonstrated that different metabolic pathways have adverse effect on lung inflammation during SARS-CoV-2 infection (Xiao et al., 2021). In TPC3, most of enriched pathways were correlated to immune response, like RIG-I-like receptor signaling. These responses were intrigued dramatically at early phase and sustained during the viral infection. PI3K-Akt pathway, ECM-receptor interaction and focal adhesion in TPC1 were mainly activated at 4 and 6 dpi.

To investigate the kinase activity and their regulation in cell signals, we integrated all kinases that were dysregulated in transcriptome, proteome and phosphoproteome. Only two kinases, CDK1 and TTN, are perturbed in all three omics (Figure 6E and Table S1). TTN, a key component in regulating muscle construction, is also associated with mitosis in non-muscle cells. CDK1 plays a vital role in controlling cell cycle and has extensive functions in cell proliferation and organ regeneration. To further analyze the underlying interaction of DE kinases, we retrieved the upstream signals and substrates of kinases in Table S1 from PhosphoSitePlus (<https://www.phosphosite.org>). We found that CDK1 regulates the phosphorylation of many other kinases, including AAK1, AKAP12, MAPK3, MASTL, NME2, CDKN1A, CDKN1B, PBK, PI3KC2A, PI4KB, PKN1, PKN2 and TTK, which were also dysregulated in our data. Wee1 is the upstream signal of CDK1, and could be phosphorylated by PLK1, which is mediated by MAPKAPK2, STK10 and Aurka. MAPKAPK2

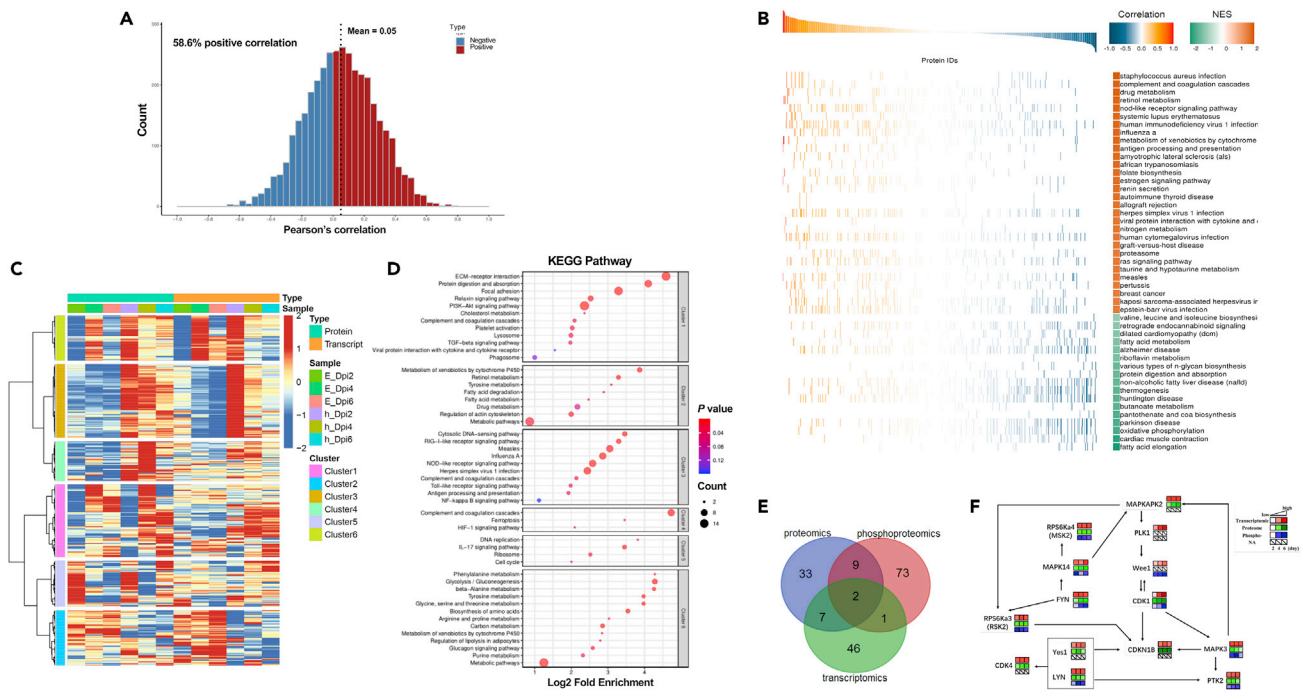


Figure 6. Integrative analysis of transcriptome, proteome and phosphoproteome of lung tissues from sensitized mice upon SARS-CoV-2 infection
 (A) Cumulative distribution of Pearson's correlation coefficient between transcriptome and proteome.
 (B) Pathway enrichment based on the correlation coefficient between differentially expressed genes and proteins through gene set enrichment analysis (GSEA). NES, normalized enrichment score.
 (C) Clusters of proteins and transcripts are both dysregulated upon SARS-CoV-2 infection.
 (D) Pathway enrichment of DE proteins from (C) by KEGG analysis.
 (E) Venn diagram of DE kinases from transcriptome, proteome and phosphoproteome.
 (F) Kinase-to-kinase network upon SARS-CoV-2 infection.
 Black lines with arrow indicate phosphorylating the downstream substrate. TPC, transcriptome and proteome cluster.

can be phosphorylated by MAPK3 and MAPK14. As one of the downstream substrates of CDK1, CDKN1B can also be phosphorylated by MAPK3, Yes1, LYN and RPS6Ka3. Notably, CDK1 also plays a regulatory role in the activation of MAPK3. We summarized these interactive kinases, and revealed the underlying regulating network of CDK and MAPK family (Figure 6F). The circuit of this kinase-to-kinase network revealed the mutual feedback relationship among CDK family and MAPK pathway.

Multiplexed quantification of SARS-CoV-2 infected mouse lung implicated dynamical regulations of lung immunology, fibrosis and mucus secretion

For the three omics data of the SARS-CoV-2 infected mouse lung at different infected time, we further screened out dysregulated signaling pathways correlated to the lung immunology, pulmonary fibrosis (PF) and mucus secretion according to previous reports. The types and enrichment level of pathways from each omics and each infection period were differentially altered (Figures S5, S6, and S7). p53 signaling pathway was prominently dysregulated in transcriptome at all time points and was associated with lung immunology and PF upon viral infection; while IL-17 signaling pathway has been involved in all the three pathological changes. For the immune response to SARS-CoV-2 (Figure S5), pathways like cytosolic DNA-sensing pathway, leukocyte transendothelial migration as well as antigen processing and presentation were continuously perturbed during viral infection, indicating the persistence of SARS-CoV-2 infection from 2 to 6 dpi. Complement and coagulation cascades belong to innate immunity, and were highly enriched at 2 and 4 dpi, while less prominent at 6 dpi. Dysregulation of adaptive immunological pathways like T cell and B cell receptor pathways was not as significant as others, probably due to the lower proportion of immune cells in the lung tissue than in other samples such as peripheral blood. PF related signaling pathways such as IL-17, p53 and PPAR pathway were significantly enriched in transcriptome of all time points (Figure S6). The rich factor of the latter two pathways continued to elevate at 6 dpi. Since PF was a late-onset complication in the COVID-19, we assumed that p53 and PPAR signaling pathway were

more correlated to its development. In accordance, we found that ferroptosis did not significantly perturb until 4 and 6 dpi, and ECM-receptor interaction only came up at 6 dpi, showing that they might be the vital pathways mediating the pathogenesis of PF upon SARS-CoV-2 infection. For mucus secretion (Figure S7), signaling pathways like IL-17, Chemokine, TNF and ErbB signaling pathway were consistently dysregulated at all time points, but we also noticed that some pathways were predominant at late phase, such as salivary secretion, glycosphingolipid biosynthesis and glycosaminoglycan biosynthesis, probably explaining the exaggeration of mucus production and secretion at late stage of infection.

DISCUSSION

Previous descriptive studies have left vacancy on the temporal regulation of lung pathophysiology during SARS-CoV-2 infection. Our multi-omics analysis showed a dynamical perturbation on the transcription, translation and phosphorylation processes in mouse lung during SARS-CoV-2 infection. The dysregulated transcripts, proteins and phosphopeptides were enriched in signaling cascades regarding cell metabolism, immunity, tissue injury and wound healing response, and so on. And many dysregulated pathways revealed in this model were accordant to what were found in COVID-19 patients, e.g. Complement and coagulation cascades and Platelet activation (Jain et al., 2020; Suvarna et al., 2021), suggesting that our study has a referential meaning for the COVID-19.

Facing a novel deadly virus, it is important for us to know whether it shares common pathogenic mechanisms with other viruses or it has unique mechanisms. We found that the pathways and signal cascades explored in this study are not specific in SARS-CoV-2 infection, since they can be dysregulated upon other kinds of infection (Kimura et al., 2013; Li and Tang, 2021; Huang and Tang, 2021). We also revealed that SARS-CoV-2 infection shared some dysregulated genes/proteins with other viral infection (e.g., Influenza, HIV, Epstein-Barr virus and human simplex virus infection) and even bacterial infection (e.g., *Staphylococcus aureus* infection). However, from another perspective, we may consider it to be a characteristic for COVID-19 that almost all the classic infectious and inflammatory pathways have participated in its disease pathogenesis. Although most of the signal cascades have been reported previously in other samples of SARS-CoV-2 infection, the main purpose of this study is to elucidate the dynamical regulation of host responses upon SARS-CoV-2 infection, which is not fully understood. By identifying the dysregulated molecules and pathways at different stages of infection as well as correlating them with pathological changes emerging at the same time, we could not only better understand the pathogenesis of COVID-19, but also explore the potential regulation mechanisms.

We showed that host metabolism was quickly intrigued at the early stage of infection. Upregulated cell metabolism provides energies and materials for viral replication and other biological processes. SARS-CoV-2 could reprogram the host metabolism to promote the expression of viral RNA and proteins (Zhang et al., 2021). Metabolic pathways have divided roles in regulating SARS-CoV-2 infection-induced systematic inflammation. For instance, inhibition of tryptophan metabolism reduced production of IL-1 α , IL-1 β and IL-6 in SARS-CoV-2 infected cells, while blocking purine metabolism brought an opposite outcome (Xiao et al., 2021). We found that purine metabolism was significantly induced at 2 dpi while downregulated at 4 and 6 dpi. Thus, the formation of inflammatory storm in severe COVID-19 might be partially ascribed to the suppression of purine metabolism at the late phase of infection.

Accompanied with the rapid metabolic response, innate immunity was also activated from the early stage of SARS-CoV-2 infection, indicated by activation of pathways regarding pathogen recognition, cytokine production, chemokines signaling pathways, complement and coagulation cascades and neutrophil degranulation. These pathways were then gradually downregulated while adaptive immune responses such as T cell, B cell, and T helper cell signaling were induced at late phase (4–6 dpi). For the underlying regulation mechanism of lung immunity upon SARS-CoV-2 infection, we proposed that CDKs and MAPK pathway may play essential roles in the activation of immune system and mediating the shift from innate immunity to adaptive immunity. Kinases of CDK and MAPK family were predominantly dysregulated during SARS-CoV-2 infection. CDKs were mainly activated at early phase while MAPK pathway was intrigued throughout the whole course. Although previous studies have evidenced the cross-interaction between MAPK and CDK and emphasized its important role in cell cycle of yeasts (Repetto et al., 2018; Durandau and Pelet, 2021), we identified this relationship in mammals with SARS-CoV-2 infection, which has been scarcely demonstrated before. What's more, we proposed that the cross-interaction between these kinases may not only function in cell cycle, but also get involved in other host responses during SARS-CoV-2 infection, such as immune response. CDKs can

regulate type I interferon (IFN) expression (Cingöz and Goff, 2018), which was produced by innate immune cells following viral infection. Besides, CDK5 and CDK8 may promote lung inflammation by inhibiting anti-inflammatory response like IL-10 production (Arif et al., 2011; Johannessen et al., 2017). MAPK pathway is involved in various immunological signaling cascades, including NF- κ B, Toll-like receptor, IL-6 receptor, and T/B cell receptor signaling (Huang et al., 2009). Many scientists have proposed MAPK pathway as a potential therapeutic target for SARS-CoV-2 infection (Grimes and Grimes, 2020), evidenced by the anti-viral effect of MAPK pathway inhibitors in SARS-CoV-2 infected cells (Bouhaddou et al., 2020; Klann et al., 2020). However, whether these inhibitors reduce lung inflammation or other pathological changes remains uncertain, so that more evidences from *in vivo* animal studies are still needed.

SARS-CoV-2 infection-associated PF is a complication and sequela of COVID-19 pneumonia, especially in severe cases, while the mechanism is still vague. In this study, we observed dysregulation of collagen deposition related proteins (e.g., Mmp9, Col5a2, Col8a2, Col11a2), indicating the emergence of lung fibrosis in our mouse model. The biological pathways in COVID-related PF were different from those of PF caused by other reasons (Yang et al., 2021). The pathogenesis of PF is associated with many factors, including cellular senescence, oxidative stress, inflammation and mitochondrial dysfunction (Yue and Yao, 2016). p53 signaling is a classic pathway regulating cell cycle and cellular senescence, triggered by various stimuli including DNA damage, inflammation storm and oxidative stress (Mijit et al., 2020). P53 expression was increased in ATI cells after lung injury, and its deficiency could block PF development, probably through hindering p53 from interacting with the fibrinolytic system (e.g., uPA, uPAR, PAI-1) (Bhandary et al., 2012, 2013). Inflammation is another crucial contributor of PF. Some profibrotic cytokines were also increased in COVID-19 patients, including IL-1 β , IL-2, IL-6, IL-8, IL-9, IL-10, IL-12 and IL-17A (She et al., 2021; Huang et al., 2020). Insufficient autophagy, marked by the accumulation of p62 and ubiquitinated proteins (Komatsu et al., 2007), is also considered as a risk factor for PF (Araya et al., 2013). In our study, p53 and IL-17 signaling pathways were continuously dysregulated. We also found that autophagy was hindered at early and middle stage post infection, indicating the delayed activated and insufficient autophagy in our mouse model. TGF- β signaling was also activated in our study, consistent with an increased TGF- β level in serum of COVID-19 patients (Agrati et al., 2020). These evidences suggested the latent roles of p53, IL-17 and TGF- β pathways as well as insufficient autophagy in the development of PF in COVID-19. A recent study revealed that TGF- β interacts with the viral protein ORF8 and promotes viral replication in human alveolar epithelial cell line A549 (Stukalov et al., 2021), while how far it affects the development of COVID-19-related PF has not been depicted. Further studies using animal models of SARS-CoV-2 induced PF need to be conducted to verify the mechanisms of COVID-19 related PF.

Excessive mucus production may be fatal through forming mucus plugs in the distal airway and leading to hypoxia in COVID-19 patients. There is a dearth of evidence on the underlying mechanism of mucus hypersecretion upon SARS-CoV-2 infection. Airway mucus production can be triggered by numerous stimuli, including microbial infection, aeroallergens, cigarette smoke, pollutants and inflammatory cytokines via activating JAK-STAT and MAPK pathways (Rose and Voynow, 2006; Khan et al., 2021; Li and Tang, 2021). Inflammation has an established role in inducing mucus production in many airway diseases (Fahy and Dickey, 2010). Liu et al. found that IFN pathways upregulated mucin proteins upon SARS-CoV-2 infection (Liu et al., 2020a). Cytokines such as IL-2, IL-4, IL-6, IL-13, IL-17 and TNF α , which were also elevated in COVID-19 patients (Huang et al., 2020), can lead to the increased production of MUC2/5AC/5B (Khan et al., 2021). Notably, unlike other cytokines, mucus production induced by IL-17 was independent of JAK-STAT signaling (Newcomb et al., 2013), implicating that JAK-STAT inhibitors might not effectively ameliorate mucus hypersecretion in COVID-19 patients (Stebbing et al., 2021). Our current study demonstrated that activation of TNF and IL-17 signaling pathways were predominant during SARS-CoV-2 infection, indicating their pivotal roles in regulating airway mucus secretion in COVID-19. Kinases such as PCTAIRE 1 and PKG2 are correlated to extracellular secretion (Palmer et al., 2005; Golin-Bisello et al., 2005), and were also activated in our study, thus may regulate excessive mucus secretion in SARS-CoV-2 infected lungs. Although TNF and IL-17 signaling pathway were activated since the early stage, the biological processes of glycoprotein synthesis and mucus secretion were induced later. This pattern of mucus production and secretion might promote rapid mucus accumulation and mucus plug formation.

In conclusion, we used multi-level omics analysis to characterize the pathological changes in mouse lungs upon SARS-CoV-2 infection. We observed predominant dysregulated signaling pathways that may explain the immune response, mucus overproduction and pulmonary fibrosis induced by SARS-CoV-2 infection, and also provide some valuable information for therapeutic development. In this study, we highlight the

feedback relationship between CDK and MAPK family, and their central roles in regulating viral replication and host immune response. Metabolic pathways like purine metabolism are involved in modulating SARS-CoV-2 induced inflammation. p53, IL-17 and TGF- β pathways as well as insufficient autophagy are closely correlated to the development of COVID-19 related PF. IL-17 and TNF pathway, as well as certain kinases like PCTAIRE 1 and PKG2 may be responsible for airway mucus hypersecretion. These factors and pathways may serve as potential biomarkers for disease course monitoring and therapeutic targets as well as increase our understanding on the pathophysiology of COVID-19.

Limitations of the study

There were some limitations of our study. First, we used a mouse model which may not totally reflect the pathological changes in human. However, the strength of using animal model is that we can serially collect samples of different infection time, while it is very difficult to acquire lung tissues from patients during the disease course. Second, in this multi-omics analysis, as all cells have been mixed and homogenized, we could hardly identify the origins of the DE transcripts and proteins. Further, studies such as single-cell sequencing on lung samples of SARS-CoV-2 infection are necessary to determine cell-specific biological perturbances.

STAR★METHODS

Detailed methods are provided in the online version of this paper and include the following:

- KEY RESOURCES TABLE
- RESOURCE AVAILABILITY
 - Lead contact
 - Materials availability
 - Data and code availability
- EXPERIMENTAL MODEL AND SUBJECT DETAILS
 - Mice
 - Virus
- METHOD DETAILS
 - Transduction and infection of mice
 - RNA extraction and RNA sequencing
 - Lung tissue digestion
 - TMT labeling
 - High performance liquid chromatography (HPLC) fractionation
 - Phosphorylation enrichment
 - LC-MS/MS analysis
 - Database search
 - Bioinformatic analysis
- QUANTIFICATION AND STATISTICAL ANALYSIS

SUPPLEMENTAL INFORMATION

Supplemental information can be found online at <https://doi.org/10.1016/j.isci.2022.103967>.

ACKNOWLEDGMENTS

This work was supported by the National High-Level Talents Program (XT), the National Natural Science Foundation of China (81770015, XT), Special Fund for Science and Technology Innovation of Guangdong Province (2020B1111330001), Guangzhou Institute of Respiratory Health Open Project (funds provided by China Evergrande Group)-Project No. 2020GIRHHMS16 and S24, Local Innovative and Research Teams Project of Guangdong Pearl River Talents Program (2017BT01S155), and Open Project of State Key Laboratory of Respiratory Disease (SKLRD-OP-202109).

AUTHOR CONTRIBUTIONS

X.X.T. conceived, designed and supervised the study. X.X.T., Z.N.W., and X.S.Y. analyzed the data. J.S. and J.C.Z. contributed to animal model and specimen collection. X.X.T. and Z.N.W. interpreted the data and wrote the manuscript. N.S.Z. critically reviewed the manuscript. All authors have read and approved the manuscript.

DECLARATION OF INTERESTS

The authors declare no competing interests.

Received: October 9, 2021

Revised: January 4, 2022

Accepted: February 17, 2022

Published: March 18, 2022

REFERENCES

- Abdala-Valencia, H., Kountz, T.S., Marchese, M.E., and Cook-Mills, J.M. (2018). VCAM-1 induces signals that stimulate ZO-1 serine phosphorylation and reduces ZO-1 localization at lung endothelial cell junctions. *J. Leukoc. Biol.* 104, 215–228. <https://doi.org/10.1002/JLB.2MA1117-427RR>.
- Agrati, C., Sacchi, A., Bordoni, V., Cimini, E., Notari, S., Grassi, G., Casetti, R., Tartaglia, E., Lalle, E., D'Abramo, A., et al. (2020). Expansion of myeloid-derived suppressor cells in patients with severe coronavirus disease (COVID-19). *Cell Death Differ.* 27, 3196–3207. <https://doi.org/10.1038/s41418-020-0572-6>.
- Anderson, R.D., Haskell, R.E., Xia, H., Roessler, B.J., and Davidson, B.L. (2000). A simple method for the rapid generation of recombinant adenovirus vectors. *Gene Ther.* 7, 1034–1038.
- Araya, J., Kojima, J., Takasaka, N., Ito, S., Fujii, S., Hara, H., Yanagisawa, H., Kobayashi, K., Tsurushige, C., Kawaishi, M., et al. (2013). Insufficient autophagy in idiopathic pulmonary fibrosis. *Am. J. Physiol. Lung Cell. Mol. Physiol.* 304, L56–L69. <https://doi.org/10.1152/ajplung.00213.2012>.
- Arif, A., Jia, J., Moodt, R.A., DiCorleto, P.E., and Fox, P.L. (2011). Phosphorylation of glutamyl-prolyl tRNA synthetase by cyclin-dependent kinase 5 dictates transcript-selective translational control. *Proc. Natl. Acad. Sci. U S A* 108, 1415–1420. <https://doi.org/10.1073/pnas.1011275108>.
- Arthur, J.S., and Ley, S.C. (2013). Mitogen-activated protein kinases in innate immunity. *Nat. Rev. Immunol.* 13, 679–692. <https://doi.org/10.1038/nri3495>.
- Atkinson, J.J., and Senior, R.M. (2003). Matrix metalloproteinase-9 in lung remodeling. *Am. J. Respir. Cell Mol. Biol.* 28, 12–24. <https://doi.org/10.1165/rcmb.2002-0166TR>.
- Balachandran, S., Roberts, P.C., Brown, L.E., Truong, H., Pattnaik, A.K., Archer, D.R., and Barber, G.N. (2000). Essential role for the dsRNA-dependent protein kinase PKR in innate immunity to viral infection. *Immunity* 13, 129–141. [https://doi.org/10.1016/s1074-7613\(00\)00014-5](https://doi.org/10.1016/s1074-7613(00)00014-5).
- Basnet, R., Gong, G.Q., Li, C., and Wang, M.W. (2018). Serum and glucocorticoid inducible protein kinases (SGKs): a potential target for cancer intervention. *Acta. Pharm. Sin. B* 8, 767–771. <https://doi.org/10.1016/j.apsb.2018.07.001>.
- Bhandary, Y.P., Shetty, S.K., Marudamuthu, A.S., Gyetko, M.R., Idell, S., Gharaee-Kermani, M., Shetty, R.S., Starcher, B.C., and Shetty, S. (2012). Regulation of alveolar epithelial cell apoptosis and pulmonary fibrosis by coordinate expression of components of the fibrinolytic system. *Am. J. Physiol. Lung Cell. Mol. Physiol.* 302, L463–L473. <https://doi.org/10.1152/ajplung.00099.2011>.
- Bhandary, Y.P., Shetty, S.K., Marudamuthu, A.S., Ji, H.L., Neuenschwander, P.F., Boggaram, V., Morris, G.F., Fu, J., Idell, S., and Shetty, S. (2013). Regulation of lung injury and fibrosis by p53-mediated changes in urokinase and plasminogen activator inhibitor-1. *Am. J. Pathol.* 183, 131–143. <https://doi.org/10.1016/j.ajpath.2013.03.022>.
- Bindea, G., Mlecnik, B., Hackl, H., Charoentong, P., Tosolini, M., Kirilovsky, A., Fridman, W.H., Pagès, F., Trajanoski, Z., and Galon, J. (2009). ClueGO: a Cytoscape plug-in to decipher functionally grouped gene ontology and pathway annotation networks. *Bioinformatics* 25, 1091–1093. <https://doi.org/10.1093/bioinformatics/btp101>.
- Borcuzuk, A.C., Salvatore, S.P., Seshan, S.V., Patel, S.S., Bussell, J.B., Mostyka, M., Elsoukkary, S., He, B., Del Vecchio, C., Fortarezza, F., et al. (2020). COVID-19 pulmonary pathology: a multi-institutional autopsy cohort from Italy and New York City. *Mod. Pathol.* 33, 2156–2168. <https://doi.org/10.1038/s41379-020-00661-1>.
- Bouhaddou, M., Memon, D., Meyer, B., White, K.M., Rezelj, V.V., Correa Marrero, M., Polacco, B.J., Melnyk, J.E., Ulferts, S., Kaake, R.M., et al. (2020). The global phosphorylation landscape of SARS-CoV-2 infection. *Cell* 182, 685–712.e19. <https://doi.org/10.1016/j.cell.2020.06.034>.
- Brunet, A., Park, J., Tran, H., Hu, L.S., Hemmings, B.A., and Greenberg, M.E. (2001). Protein kinase SGK mediates survival signals by phosphorylating the forkhead transcription factor FKHL1 (FOXO3a). *Mol. Cell. Biol.* 21, 952–965. <https://doi.org/10.1128/MCB.21.3.952-965.2001>.
- Carsana, L., Sonzogni, A., Nasr, A., Rossi, R.S., Pellegrinelli, A., Zerbi, P., Rech, R., Colombo, R., Antinori, S., Corbellino, M., et al. (2020). Pulmonary post-mortem findings in a series of COVID-19 cases from northern Italy: a two-centre descriptive study. *Lancet Infect. Dis.* 20, 1135–1140. [https://doi.org/10.1016/S1473-3099\(20\)30434-5](https://doi.org/10.1016/S1473-3099(20)30434-5).
- Cingöz, O., and Goff, S.P. (2018). Cyclin-dependent kinase activity is required for type I interferon production. *Proc. Natl. Acad. Sci. U S A* 115, E2950–E2959. <https://doi.org/10.1073/pnas.1720431115>.
- Cheng, A., Grant, C.E., Noble, W.S., and Bailey, T.L. (2019). MoMo: discovery of statistically significant post-translational modification motifs. *Bioinformatics* 35, 2774–2782. <https://doi.org/10.1093/bioinformatics/bty1058>.
- Deretic, V., Saitoh, T., and Akira, S. (2013). Autophagy in infection, inflammation and immunity. *Nat. Rev. Immunol.* 13, 722–737.
- Doyle, S.L., Jefferies, C.A., Feighery, C., and O'Neill, L.A. (2007). Signaling by Toll-like receptors 8 and 9 requires Bruton's tyrosine kinase. *J. Biol. Chem.* 282, 36953–36960. <https://doi.org/10.1074/jbc.M707682200>.
- Durandau, E., and Pelet, S. (2021). Cross-regulation between CDK and MAPK control cellular fate. *Quant. Biol.* 9, 341–359. <https://doi.org/10.15302/J-QB-021-0240>.
- Fahy, J.V., and Dickey, B.F. (2010). Airway mucus function and dysfunction. *N. Engl. J. Med.* 363, 2233–2247. <https://doi.org/10.1056/NEJMr0910061>.
- Gassen, N., Papiés, J., Bajaj, T., Dethloff, F., Emanuel, J., Weckmann, K., Heinz, D.E., Heinemann, N., Lennarz, M., Richter, A., et al. (2020). Analysis of SARS-CoV-2-controlled autophagy reveals spermidine, MK-2206, and niclosamide as putative antiviral therapeutics. *bioRxiv*. <https://doi.org/10.1101/2020.04.15.997254>.
- Gerbe, F., Sidot, E., Smyth, D.J., Ohmoto, M., Matsumoto, I., Dardalhon, V., Cesses, P., Garnier, L., Pouzolles, M., Brulin, B., et al. (2016). Intestinal epithelial tuft cells initiate type 2 mucosal immunity to helminth parasites. *Nature* 529, 226–230. <https://doi.org/10.1038/nature16527>.
- Golin-Bisello, F., Bradbury, N., and Ameen, N. (2005). STa and cGMP stimulate CFTR translocation to the surface of villus enterocytes in rat jejunum and is regulated by protein kinase G. *Am. J. Physiol. Cell Physiol.* 289, C708–C716. <https://doi.org/10.1152/ajpcell.00544.2004>.
- Grimes, J.M., and Grimes, K.V. (2020). p38 MAPK inhibition: a promising therapeutic approach for COVID-19. *J. Mol. Cell. Cardiol.* 144, 63–65. <https://doi.org/10.1016/j.yjmcc.2020.05.007>.
- Gutierrez-Chamorro, L., Felip, E., Ezeonwumelu, I.J., Margelí, M., and Ballana, E. (2021). Cyclin-dependent kinases as emerging targets for developing novel antiviral therapeutics. *Trends Microbiol.* <https://doi.org/10.1016/j.tim.2021.01.014>.
- Hancock, L.A., Hennessy, C.E., Solomon, G.M., Dobrinskikh, E., Estrella, A., Hara, N., Hill, D.B., Kissner, W.J., Markovetz, M.R., Grove Villalon, D.E., et al. (2018). Muc5b overexpression causes mucociliary dysfunction and enhances lung fibrosis in mice. *Nat. Commun.* 9, 5363. <https://doi.org/10.1038/s41467-018-07768-9>.
- He, J., Cai, S., Feng, H., Cai, B., Lin, L., Mai, Y., Fan, Y., Zhu, A., Huang, H., Shi, J., et al. (2020).

- Single-cell analysis reveals bronchoalveolar epithelial dysfunction in COVID-19 patients. *Protein Cell* 11, 680–687. <https://doi.org/10.1007/s13238-020-00752-4>.
- Hoeflich, K.P., Luo, J., Rubie, E.A., Tsao, M.S., Jin, O., and Woodgett, J.R. (2000). Requirement for glycogen synthase kinase-3 β in cell survival and NF- κ B activation. *Nature* 406, 86–90. <https://doi.org/10.1038/35017574>.
- Hoffmann, M., Kleine-Weber, H., Schroeder, S., Krüger, N., Herrler, T., Erichsen, S., Schiergens, T.S., Herrler, G., Wu, N.H., Nitsche, A., et al. (2020). SARS-CoV-2 cell entry depends on ACE2 and TMPRSS2 and is blocked by a clinically proven protease inhibitor. *Cell* 181, 271–280.
- Hofmann, F., Feil, R., Kleppisch, T., and Schlossmann, J. (2006). Function of cGMP-dependent protein kinases as revealed by gene deletion. *Physiol. Rev.* 86, 1–23. <https://doi.org/10.1152/physrev.00015.2005>.
- Hooper, J.E., Padera, R.F., Dolnikoff, M., da Silva, L., Duarte-Neto, A.N., Kapp, M.E., Lacy, J.M., Mauad, T., Nascimento Saldiva, P.H., Rapkiewicz, A.V., et al. (2021). A postmortem portrait of the coronavirus disease 2019 (COVID-19) pandemic: a large multiinstitutional autopsy survey study. *Arch. Pathol. Lab. Med.* <https://doi.org/10.5858/arpa.2020-0786-SA>.
- Hu, J., Li, S., Sun, X., Fang, Z., Wang, L., Xiao, F., Shao, M., Ge, L., Tang, F., Gu, J., et al. (2019). *Stk40* deletion elevates c-JUN protein level and impairs mesoderm differentiation. *J. Biol. Chem.* 294, 9959–9972. <https://doi.org/10.1074/jbc.RA119.007840>.
- Huang, C., Wang, Y., Li, X., Ren, L., Zhao, J., Hu, Y., Zhang, L., Fan, G., Xu, J., Gu, X., et al. (2020). Clinical features of patients infected with 2019 novel coronavirus in Wuhan, China. *Lancet* 395, 497–506. [https://doi.org/10.1016/S0140-6736\(20\)30183-5](https://doi.org/10.1016/S0140-6736(20)30183-5).
- Huang, G., Shi, L.Z., and Chi, H. (2009). Regulation of JNK and p38 MAPK in the immune system: signal integration, propagation and termination. *Cytokine* 48, 161–169. <https://doi.org/10.1016/j.cyto.2009.08.002>.
- Huang, W.J., and Tang, X.X. (2021). Virus infection induced pulmonary fibrosis. *J. Transl. Med.* 19, 496. <https://doi.org/10.1186/s12967-021-03159-9>.
- Jain, R., Ramaswamy, S., Harilal, D., Uddin, M., Loney, T., Nowotny, N., Alsuwaidi, H., Varghese, R., Deesi, Z., Alkhajeh, A., et al. (2020). Host transcriptomic profiling of COVID-19 patients with mild, moderate, and severe clinical outcomes. *Comput. Struct. Biotechnol. J.* 19, 153–160. <https://doi.org/10.1016/j.csbj.2020.12.016>.
- Johannessen, L., Sundberg, T.B., O’Connell, D.J., Kolde, R., Berstler, J., Billings, K.J., Khor, B., Seashore-Ludlow, B., Fassl, A., Russell, C.N., et al. (2017). Small-molecule studies identify CDK8 as a regulator of IL-10 in myeloid cells. *Nat. Chem. Biol.* 13, 1102–1108. <https://doi.org/10.1038/nchembio.2458>.
- Kamemura, N., Murakami, S., Komatsu, H., Sawanoi, M., Miyamoto, K., Ishidoh, K., Kishimoto, K., Tsuji, A., and Yuasa, K. (2017). Type II cGMP-dependent protein kinase negatively regulates fibroblast growth factor signaling by phosphorylating Raf-1 at serine 43 in rat chondrosarcoma cells. *Biochem. Biophys. Res. Commun.* 483, 82–87. <https://doi.org/10.1016/j.bbrc.2017.01.001>.
- Kanehisa, M., Furumichi, M., Sato, Y., Ishiguro-Watanabe, M., & Tanabe, M. (2021). KEGG: integrating viruses and cellular organisms. *Nucleic Acids Res.* 49 (D1), D545–D551. <https://doi.org/10.1093/nar/gkaa970>
- Katoh, M., and Katoh, M. (2009). Integrative genomic analyses of WNT11: transcriptional mechanisms based on canonical WNT signals and GATA transcription factors signaling. *Int. J. Mol. Med.* 24, 247–251. <https://doi.org/10.3892/ijmm.00000227>.
- Khan, W.N. (2001). Regulation of B lymphocyte development and activation by Bruton’s tyrosine kinase. *Immunol. Res.* 23, 147–156. <https://doi.org/10.1385/IR:23:2:3:147>.
- Khan, M.A., Khan, Z.A., Charles, M., Pratap, P., Naeem, A., Siddiqui, Z., Naqvi, N., and Srivastava, S. (2021). Cytokine storm and mucus hypersecretion in COVID-19: review of mechanisms. *J. Inflamm. Res.* 14, 175–189. <https://doi.org/10.2147/JIR.S271292>.
- Kimura, H., Yoshizumi, M., Ishii, H., Oishi, K., and Ryo, A. (2013). Cytokine production and signaling pathways in respiratory virus infection. *Front. Microbiol.* 4, 276. <https://doi.org/10.3389/fmicb.2013.00276>.
- Klann, K., Bojkova, D., Tascher, G., Ciesek, S., Münch, C., and Cinatl, J. (2020). Growth factor receptor signaling inhibition prevents SARS-CoV-2 replication. *Mol. Cell* 80, 164–174.e4. <https://doi.org/10.1016/j.molcel.2020.08.006>.
- Kohanski, M.A., Workman, A.D., Patel, N.N., Hung, L.Y., Shtraks, J.P., Chen, B., Blasetti, M., Doghramji, L., Kennedy, D.W., Adappa, N.D., et al. (2018). Solitary chemosensory cells are a primary epithelial source of IL-25 in patients with chronic rhinosinusitis with nasal polyps. *J. Allergy Clin. Immunol.* 142, 460–469.e7. <https://doi.org/10.1016/j.jaci.2018.03.019>.
- Komatsu, M., Waguri, S., Koike, M., Sou, Y.S., Ueno, T., Hara, T., Mizushima, N., Iwata, J., Ezaki, J., Murata, S., et al. (2007). Homeostatic levels of p62 control cytoplasmic inclusion body formation in autophagy-deficient mice. *Cell* 131, 1149–1163. <https://doi.org/10.1016/j.cell.2007.10.035>.
- Kumar, L., and E Futschik, M. (2007). Mfuzz: a software package for soft clustering of microarray data. *Bioinformatics* 21, 5–7. <https://doi.org/10.6026/97320630002005>.
- Leng, L., Cao, R., Ma, J., Mou, D., Zhu, Y., Li, W., Lv, L., Gao, D., Zhang, S., Gong, F., et al. (2020). Pathological features of COVID-19-associated lung injury: a preliminary proteomics report based on clinical samples. *Signal Transduct. Target Ther.* 5, 240. <https://doi.org/10.1038/s41392-020-00355-9>.
- Li, L., Sun, L., Gao, F., Jiang, J., Yang, Y., Li, C., Gu, J., Wei, Z., Yang, A., Lu, R., et al. (2010). *Stk40* links the pluripotency factor Oct4 to the Erk/MAPK pathway and controls extraembryonic endoderm differentiation. *Proc. Natl. Acad. Sci. U S A* 107, 1402–1407. <https://doi.org/10.1073/pnas.0905657107>.
- Li, Y., and Tang, X.X. (2021). Abnormal airway mucus secretion induced by virus infection. *Front. Immunol.* 12, 701443. <https://doi.org/10.3389/fimmu.2021.701443>.
- Liu, Y., Lv, J., Liu, J., Li, M., Xie, J., Lv, Q., Deng, W., Zhou, N., Zhou, Y., Song, J., et al. (2020a). Mucus production stimulated by IFN- α H α R signaling triggers hypoxia of COVID-19. *Cell Res.* 30, 1078–1087. <https://doi.org/10.1038/s41422-020-00435-z>.
- Liu, Z., Han, M., Ding, K., and Fu, R. (2020b). The role of Pim kinase in immunomodulation. *Am. J. Cancer Res.* 10, 4085–4097.
- Miao, G., Zhao, H., Li, Y., Ji, M., Chen, Y., Shi, Y., Bi, Y., Wang, P., and Zhang, H. (2021). ORF3a of the COVID-19 virus SARS-CoV-2 blocks HOPS complex-mediated assembly of the SNARE complex required for autolysosome formation. *Dev. Cell* 56, 427–442.e5. <https://doi.org/10.1016/j.devcel.2020.12.010>.
- Mijit, M., Caracciolo, V., Melillo, A., Amicarelli, F., and Giordano, A. (2020). Role of p53 in the regulation of cellular senescence. *Biomolecules* 10, 420. <https://doi.org/10.3390/biom10030420>.
- Miller, C.N., Proekt, I., von Moltke, J., Wells, K.L., Rajpurkar, A.R., Wang, H., Rattay, K., Khan, I.S., Metzger, T.C., Pollack, J.L., et al. (2018). Thymic tuft cells promote an IL-4-enriched medulla and shape thymocyte development. *Nature* 559, 627–631. <https://doi.org/10.1038/s41586-018-0345-2>.
- Moriya, Y., Itoh, M., Okuda, S., Yoshizawa, A. C., & Kanehisa, M. (2007). KAA5: an automatic genome annotation and pathway reconstruction server. *Nucleic Acids Res.* 35 (Web Server issue), W182–W185. <https://doi.org/10.1093/nar/gkm321>.
- Newcomb, D.C., Boswell, M.G., Sherrill, T.P., Polosukhin, V.V., Boyd, K.L., Goleniewska, K., Brody, S.L., Kolls, J.K., Adler, K.B., and Peebles, R.S., Jr. (2013). IL-17A induces signal transducers and activators of transcription-6-independent airway mucous cell metaplasia. *Am. J. Respir. Cell Mol. Biol.* 48, 711–716. <https://doi.org/10.1165/rcmb.2013-0017OC>.
- Nie, X., Qian, L., Sun, R., Huang, B., Dong, X., Xiao, Q., Zhang, Q., Lu, T., Yue, L., Chen, S., et al. (2021). Multi-organ proteomic landscape of COVID-19 autopsies. *Cell*. <https://doi.org/10.1016/j.cell.2021.01.004>.
- Noth, I., Zhang, Y., Ma, S.F., Flores, C., Barber, M., Huang, Y., Broderick, S.M., Wade, M.S., Hysi, P., Scuirba, J., et al. (2013). Genetic variants associated with idiopathic pulmonary fibrosis susceptibility and mortality: a genome-wide association study. *Lancet Respir. Med.* 1, 309–317. [https://doi.org/10.1016/S2213-2600\(13\)70045-6](https://doi.org/10.1016/S2213-2600(13)70045-6).
- Noubouossie, D.F., Reeves, B.N., Strahl, B.D., and Key, N.S. (2019). Neutrophils: back in the thrombosis spotlight. *Blood* 133, 2186–2197. <https://doi.org/10.1182/blood-2018-10-862243>.
- Palmer, K.J., Konkol, J.E., and Stephens, D.J. (2005). PCTAIRE protein kinases interact directly with the COPII complex and modulate secretory cargo transport. *J. Cell Sci.* 118, 3839–3847. <https://doi.org/10.1242/jcs.02496>.

- Peng, Y., Wang, Z.N., Xu, A.R., Fang, Z.F., Chen, S.Y., Hou, X.T., Zhou, Z.Q., Lin, H.M., Xie, J.X., Tang, X.X., Wang, D.Y., and Zhong, N.S. (2022). Mucus hypersecretion and ciliary impairment in conducting airway contribute to alveolar mucus plugging in idiopathic pulmonary fibrosis. *Front. Cell Dev. Biol.* 9, 810842. <https://doi.org/10.3389/fcell.2021.810842>.
- Qu, Y., Wang, X., Zhu, Y., Wang, Y., and Liang, Q. (2020). ORF3a mediated-incomplete autophagy facilitates SARS-CoV-2 replication. *bioRxiv*. <https://doi.org/10.1101/2020.11.12.380709>.
- Repetto, M.V., Winters, M.J., Bush, A., Reiter, W., Hollenstein, D.M., Ammerer, G., Pryciak, P.M., and Colman-Lerner, A. (2018). CDK and MAPK synergistically regulate signaling dynamics via a shared multi-site phosphorylation region on the scaffold protein Ste5. *Mol Cell* 69, 938–952.e6. <https://doi.org/10.1016/j.molcel.2018.02.018>.
- Rose, M.C., and Voynow, J.A. (2006). Respiratory tract mucin genes and mucin glycoproteins in health and disease. *Physiol. Rev.* 86, 245–278. <https://doi.org/10.1152/physrev.00010.2005>.
- Sarhan, J., Liu, B.C., Muendlein, H.I., Weindel, C.G., Smirnova, I., Tang, A.Y., Ilyukha, V., Sorokin, M., Buzdin, A., Fitzgerald, K.A., and Poltorak, A. (2019). Constitutive interferon signaling maintains critical threshold of MLKL expression to license necroptosis. *Cell Death Differ.* 26, 332–347. <https://doi.org/10.1038/s41418-018-0122-7>.
- Senftleben, U., Cao, Y., Xiao, G., Greten, F.R., Krähn, G., Bonizzi, G., Chen, Y., Hu, Y., Fong, A., Sun, S.C., and Karin, M. (2001). Activation by IKK α of a second, evolutionary conserved, NF- κ B signaling pathway. *Science* 293, 1495–1499. <https://doi.org/10.1126/science.1062677>.
- Sharma, S., and Sicsinski, P. (2020). A kinase of many talents: non-neuronal functions of CDK5 in development and disease. *Open Biol.* 10, 190287. <https://doi.org/10.1098/rsob.190287>.
- She, Y.X., Yu, Q.Y., and Tang, X.X. (2021). Role of interleukins in the pathogenesis of pulmonary fibrosis. *Cell Death Discov.* 7, 52. <https://doi.org/10.1038/s41420-021-00437-9>.
- Stebbing, J., Sánchez Nieves, G., Falcone, M., Youhanna, S., Richardson, P., Ottaviani, S., Shen, J.X., Sommerauer, C., Tiseo, G., Ghiadoni, L., et al. (2021). JAK inhibition reduces SARS-CoV-2 liver infectivity and modulates inflammatory responses to reduce morbidity and mortality. *Sci. Adv.* 7, eabe4724. <https://doi.org/10.1126/sciadv.abe4724>.
- Stukalov, A., Girault, V., Grass, V., Karayel, O., Bergant, V., Urban, C., Haas, D.A., Huang, Y., Oubraham, L., Wang, A., et al. (2021). Multilevel proteomics reveals host perturbations by SARS-CoV-2 and SARS-CoV. *Nature*. <https://doi.org/10.1038/s41586-021-03493-4>.
- Sun, H., Yang, W., Tian, Y., Zeng, X., Zhou, J., Mok, M.T.S., Tang, W., Feng, Y., Xu, L., Chan, A.W.H., et al. (2018). An inflammatory-CRCR circuitry drives mTORC1-dependent metabolic and immunosuppressive reprogramming in obesity-associated hepatocellular carcinoma. *Nat. Commun.* 9, 5214. <https://doi.org/10.1038/s41467-018-07402-8>.
- Sun, J., Zhuang, Z., Zheng, J., Li, K., Wong, R.L., Liu, D., Huang, J., He, J., Zhu, A., Zhao, J., et al. (2020). Generation of a broadly useful model for COVID-19 pathogenesis, vaccination, and treatment. *Cell* 182, 734–743.e5. <https://doi.org/10.1016/j.cell.2020.06.010>.
- Suvarna, K., Salkar, A., Palanivel, V., Bankar, R., Banerjee, N., Gayathri J Pai, M., Srivastava, A., Singh, A., Khatri, H., Agrawal, S., et al. (2021). A multi-omics longitudinal study reveals alteration of the leukocyte activation pathway in COVID-19 patients. *J. Proteome Res.* 20, 4667–4680.
- Szklarczyk, D., Gable, A.L., Lyon, D., Junge, A., Wyder, S., Huerta-Cepas, J., Simonovic, M., Doncheva, N.T., Morris, J.H., Bork, P., et al. (2019). STRING v11: protein-protein association networks with increased coverage, supporting functional discovery in genome-wide experimental datasets. *Nucleic Acids Res.* 47, D607–D613. <https://doi.org/10.1093/nar/gky1131>.
- Taccioli, C., Garofalo, M., Chen, H., Jiang, Y., Tagliacruzchi, G.M., Di Leva, G., Alder, H., Fadda, P., Middleton, J., Smalley, K.J., et al. (2015). Repression of esophageal neoplasia and inflammatory signaling by anti-miR-31 delivery in vivo. *J. Natl. Cancer Inst.* 107, djv220. <https://doi.org/10.1093/jnci/djv220>.
- Tian, S., Xiong, Y., Liu, H., Niu, L., Guo, J., Liao, M., and Xiao, S.Y. (2020). Pathological study of the 2019 novel coronavirus disease (COVID-19) through postmortem core biopsies. *Mod. Pathol.* 33, 1007–1014. <https://doi.org/10.1038/s41379-020-0536-x>.
- Tyanova, S., Temu, T., and Cox, J. (2016). The MaxQuant computational platform for mass spectrometry-based shotgun proteomics. *Nat. Protoc.* 11, 2301–2319. <https://doi.org/10.1038/nprot.2016.136>.
- Wang, R., Kwon, I.K., Thangaraju, M., Singh, N., Liu, K., Jay, P., Hofmann, F., Ganapathy, V., and Browning, D.D. (2012). Type 2 cGMP-dependent protein kinase regulates proliferation and differentiation in the colonic mucosa. *Am. J. Physiol. Gastrointest Liver Physiol.* 303, G209–G219. <https://doi.org/10.1152/ajpgi.00500.2011>.
- Wu, M., Chen, Y., Xia, H., Wang, C., Tan, C.Y., Cai, X., Liu, Y., Ji, F., Xiong, P., Liu, R., et al. (2020). Transcriptional and proteomic insights into the host response in fatal COVID-19 cases. *Proc. Natl. Acad. Sci. U S A* 117, 28336–28343. <https://doi.org/10.1073/pnas.2018030117>.
- Xiao, N., Nie, M., Pang, H., Wang, B., Hu, J., Meng, X., Li, K., Ran, X., Long, Q., Deng, H., et al. (2021). Integrated cytokine and metabolite analysis reveals immunometabolic reprogramming in COVID-19 patients with therapeutic implications. *Nat. Commun.* 12, 1618. <https://doi.org/10.1038/s41467-021-21907-9>.
- Yang, F., Chen, R., Li, W.Y., Zhu, H.Y., Chen, X.X., Hou, Z.F., Cao, R.S., Zang, G., Li, Y.X., and Zhang, W. (2021). D-limonene is a potential monoterpene to inhibit PI3K/Akt/IKK- α /NF- κ B p65 signaling pathway in coronavirus disease 2019 pulmonary fibrosis. *Front. Med.* 8, 591830. <https://doi.org/10.3389/fmed.2021.591830>.
- Yang, C., Li, L., Guo, J., Zhang, W., Zhu, W., Rao, X., and Huang, W. (2017). Up-regulation of Pim-3 in Chronic Obstructive Pulmonary Disease (COPD) patients and its potential therapeutic role in COPD rat modeling. *Pathol. Res. Pract.* 213, 322–326. <https://doi.org/10.1016/j.prp.2017.01.018>.
- Yang, J., Li, X., Hanidu, A., Htut, T.M., Sellati, R., Wang, L., Jiang, H., and Li, J. (2010). Proviral integration site 2 is required for interleukin-6 expression induced by interleukin-1, tumour necrosis factor- α and lipopolysaccharide. *Immunology* 131, 174–182. <https://doi.org/10.1111/j.1365-2567.2010.03286.x>.
- Yu, C.S., Lin, C.J., and Hwang, J.K. (2004). Predicting subcellular localization of proteins for Gram-negative bacteria by support vector machines based on n-peptide compositions. *Protein Sci.* 13, 1402–1406. <https://doi.org/10.1110/ps.03479604>.
- Yue, L., and Yao, H. (2016). Mitochondrial dysfunction in inflammatory responses and cellular senescence: pathogenesis and pharmacological targets for chronic lung diseases. *Br. J. Pharmacol.* 173, 2305–2318. <https://doi.org/10.1111/bph.13518>.
- Zaki, A.M., van Boheemen, S., Bestebroer, T.M., Osterhaus, A.D., and Fouchier, R.A. (2012). Isolation of a novel coronavirus from a man with pneumonia in Saudi Arabia. *N. Engl. J. Med.* 367, 1814–1820.
- Zhang, Y., Guo, R., Kim, S.H., Shah, H., Zhang, S., Liang, J.H., Fang, Y., Gentili, M., Leary, C.N.O., Elledge, S.J., et al. (2021). SARS-CoV-2 hijacks folate and one-carbon metabolism for viral replication. *Nat. Commun.* 12, 1676. <https://doi.org/10.1038/s41467-021-21903-z>.
- Zhong, N.S., Zheng, B.J., Li, Y.M., Poon, Z.H., Xie, Z.H., Chan, K.H., Li, P.H., Tan, S.Y., Chang, Q., Xie, J.P., et al. (2003). Epidemiology and cause of severe acute respiratory syndrome (SARS) in Guangdong, People's Republic of China, in February, 2003. *Lancet* 362, 1353–1358.
- Zhou, Y., Zhou, B., Pache, L., Chang, M., Khodabakhshi, A.H., Tanaseichuk, O., Benner, C., and Chanda, S.K. (2019). Metascape provides a biologist-oriented resource for the analysis of systems-level datasets. *Nat. Commun.* 10, 1523. <https://doi.org/10.1038/s41467-019-09234-6>.

STAR★METHODS

KEY RESOURCES TABLE

REAGENT or RESOURCE	SOURCE	IDENTIFIER
Bacterial and virus strains		
SARS-CoV-2/human/CHN/IQTC01/2020 (GenBank: MT123290.1)		N/A
Chemicals, peptides, and recombinant protein		
DMEM	GIBCO	Cat.# C11965500BT
Typsin	Promega	Cat # V5111
Triethylammonium bicarbonate buffer (TEAB)	Sigma-Aldrich	Cat # T7408
Urea	Sigma-Aldrich	Cat # U1250
Protease and Phosphatase Inhibitor Cocktail	Thermo Fisher Scientific	Cat # 78442
BCA kit	Thermo Fisher Scientific	Cat # 23250
Dithiothreitol	Sigma-Aldrich	Cat # 43815
Iodoacetamide	Sigma-Aldrich	Cat # I6125
Strata X C18	Phenomenex	Cat # 8B-S100
Trifluoroacetic acid	Sigma-Aldrich	Cat # T6508
Acetonitrile	Fisher Chemical	Cat # LS120
Formic acid	Fluka	Cat # 27001
Critical commercial assays		
TMTsixplex™ Isobaric Label Reagent Set	Thermo Fisher Scientific	Cat # 90068
RNeasy mini kit	Qiagen	Cat # 74104
TruSeq™ RNA Sample Preparation Kit	Illumina	Cat # RS-122-2001
Deposited data		
Mass spectrometry data	PRIDE	PXD031574
RNA sequence data	GEO	GSE196488
Experimental models: Organisms/strains		
Mouse: WT BALB/c mouse	Hunan SJA Laboratory Animal Co.(China)	N/A
Software and algorithms		
Maxquant (version 1.5.2.8)	Tyanova et al. (2016)	http://www.maxquant.org/
STRING (v.11.0)	Szklarczyk et al., (2019)	https://string-db.org/
R version 3.6.1	R Project	https://www.r-project.org
Metascape	Zhou et al. (2019)	https://metascape.org/gp/index.html#/main/step1
ClueGO 2.5.6	Bindea et al. (2009)	https://cytoscape.org/
MoMo (v.5.0.2)	Cheng et al. (2019)	http://meme-suite.org/tools/momo
InterProScan (v.5.14-53.0)	the European Bioinformatics Institute in Cambridge	http://www.ebi.ac.uk/interpro/
KAAS (v.2.0)	Moriya et al. (2007)	http://www.genome.jp/kaas-bin/kaas_main
KEGG Mapper (v.2.5)	Kanehisa et al. (2021)	http://www.kegg.jp/kegg/mapper.html
Wolfsort (v.0.2)	Computational Biology Research Center	http://www.genscript.com/psort/wolf_psort.html
CELLO (v.2.5)	Yu et al. (2004)	http://cello.life.nctu.edu.tw/
Blast (v.2.2.26)	National Center for Biotechnology Information	http://blast.ncbi.nlm.nih.gov/Blast.cgi

(Continued on next page)

Continued

REAGENT or RESOURCE	SOURCE	IDENTIFIER
Other		
Qubit® 2.0 Fluorometer	Life Technologies	N/A
Agilent 2100 bioanalyzer	Agilent Technologies	N/A
Illumina NovaSeq 6000	Illumina	N/A
Hisat2 (v.2.0.5)	Hierarchical Indexing for Spliced Alignment of Transcripts	https://github.com/trinityrnaseq/trinityrnaseq/wiki

RESOURCE AVAILABILITY

Lead contact

Further information should be directed to and will be fulfilled by the Lead Contact, Xiao Xiao Tang (tangxiaoxiao@gird.cn).

Materials availability

This study did not generate new unique reagents.

Data and code availability

RNA sequences and mass spectrometry data have been deposited at GEO and PRIDE, respectively, and are publicly available as of the date of publication. Accession codes are listed in the [key resources table](#). Other data or additional information reported in this paper is available from the lead contact upon request. This paper does not report original code.

EXPERIMENTAL MODEL AND SUBJECT DETAILS

Mice

Specific pathogen-free 6–10-week-old female BALB/c mice were purchased from Hunan SJA Laboratory Animal Co. (Hunan, China) and maintained in the Animal Care Facilities at the Guangzhou Medical University. All protocols have been approved by the Institutional Animal Care and Use Committees of the Guangzhou Medical University.

Virus

The SARS-CoV-2 strain used in this study was isolated from COVID-19 patients in Guangzhou (Accession numbers: MT123290), and passaged on African Green monkey kidney-derived Vero E6 cells. The human serotype 5 adenoviral vector expressing human ACE2 (Ad-hACE2) under the control of the CMV promoter was generated by using the RAPAd.i system ([Anderson et al., 2000](#)).

METHOD DETAILS

Transduction and infection of mice

After being gently anesthetized with isoflurane, the mice were administrated intranasally with 2.5×10^8 FFU of Ad5-hACE2 or Ad5-Empty in a total volume of 75 μ L Dulbecco's modified Eagle's medium (DMEM, GIBCO, Grand Island, NY). Five days later, all mice were infected intranasally with SARS-CoV-2 (1×10^5 PFU) in 50 μ L DMEM. Mice were sacrificed and their lung tissues were freshly collected at 2, 4 and 6 days after infection. Each group was performed in biologically triplicates (n = 3 for each time point of each group). All work with SARS-CoV-2 was conducted in the Biosafety Level 3 (BSL3) Laboratories of Guangzhou Customs District Technology Center.

RNA extraction and RNA sequencing

Total RNA from mouse lung tissues was isolated using RNeasy mini kit (Qiagen, Germany). Paired-end libraries were synthesized by using the TruSeq™ RNA Sample Preparation Kit (Illumina, USA) following TruSeq™ RNA Sample Preparation Guide. Briefly, the poly-A containing mRNA molecules were purified using poly-T oligo-attached magnetic beads.

Following purification, the mRNA is fragmented into small pieces using divalent cations under 94°C for 8 min. The cleaved RNA fragments are copied into first strand cDNA using reverse transcriptase and random primers. This is followed by second strand cDNA synthesis using DNA Polymerase I and RNase H. These cDNA fragments then go through an end repair process, the addition of a single 'A' base, and then ligation of the adapters. The products are then purified and enriched with PCR to create the final cDNA library. Purified libraries were quantified by Qubit® 2.0 Fluorometer (Life Technologies, USA) and validated by Agilent 2100 bioanalyzer (Agilent Technologies, USA) to confirm the insert size and calculate the mole concentration. Cluster was generated by cBot with the library diluted to 10 pM and then were sequenced on the Illumina NovaSeq 6000 (Illumina, USA).

Lung tissue digestion

Samples were ground into cell powder in liquid nitrogen and four volumes of lysis buffer (8 M urea with 1× Protease and Phosphatase Inhibitor Cocktail) was added. After sonication three times on ice and centrifugation at 12,000 g at 4°C for 10 min, remaining debris was removed and the supernatant was collected. Protein concentration was determined with BCA kit (Thermo Fisher Scientific) according to the manufacturer's instructions. Protein solution was reduced with 5 mM dithiothreitol for 30 min at 56°C and alkylated with 11 mM iodoacetamide for 15 min at room temperature in darkness. The protein sample was then diluted by adding 200 mM TEAB to urea concentration less than 2M. Finally, trypsin was added at 1:50 trypsin-to-protein mass ratio for the first digestion overnight and 1:100 trypsin-to-protein mass ratio for a second 4-h digestion.

TMT labeling

Peptide digested by trypsin was desalted with Strata X C18 (Phenomenex, California, USA) and vacuum freeze-dried. Peptide was dissolved in 0.5 M TEAB (Sigma, St. Louis, MO, USA), and labeled according to the instruction of TMT kit (Thermo Scientific, Waltham, MA, USA). Briefly, the labeled reagent was thawed and dissolved in acetonitrile (ACN, Fisher Chemical, Leicestershire, UK). Then the peptide mixtures were incubated for 2 h and pooled, desalted and vacuum freeze-dried.

High performance liquid chromatography (HPLC) fractionation

The tryptic peptides were fractionated by high pH reverse-phase HPLC using Agilent 300 Extend C18 column (5 μm particles, 4.6 mm ID, 250 mm length). Briefly, peptides were first separated into 60 fractions with ACN (pH 9.0) of 8%–32% over 60 min. Then, the peptides were combined into 14 fractions and dried by vacuum centrifuging. For phosphorylation, the peptides were combined into 4 fractions and dried by vacuum centrifuging.

Phosphorylation enrichment

Peptide mixtures were first incubated with IMAC microspheres suspension with vibration in loading buffer (50% acetonitrile/0.5% acetic acid). The IMAC microspheres with enriched phosphopeptides were collected by centrifugation, and the supernatant was removed. To remove nonspecifically adsorbed peptides, the IMAC microspheres were washed with 50% acetonitrile/0.5% acetic acid and 30% acetonitrile/0.1% trifluoroacetic acid, sequentially. To elute the enriched phosphopeptides from the IMAC microspheres, elution buffer containing 10% NH₄OH was added and the enriched phosphopeptides were eluted with vibration. The supernatant containing phosphopeptides was collected and lyophilized for LC-MS/MS analysis.

LC-MS/MS analysis

Peptides dissolved in solvent A (0.1% formic acid in 2% ACN) were separated by EASY-nLC 1000 UPLC system. The gradient was comprised of an increase from 5% to 23% solvent B (0.1% FA in 90% ACN) over 40 min, 23%–35% in 12 min, 35%–80% in 4 min then holding at 80% for the last 4 min. The constant flow rate was set at 550 nL/min. The peptide was then subjected to NSI source for ionization and analyzed by QE plus mass spectrometry. The electrospray voltage applied was 2.2 kV. The m/z scan range was 350 to 1,800 for primary MS, and the resolution was set to 70,000. The fixed starting point of the scan range of secondary MS is 100 m/z, with the resolution of 35,000. Data dependent scanning (DDA) program was used as data acquisition. To enhance the efficiency of MS, automatic gain control (AGC) was set at 1E5. The signal threshold was set to 2E4 ions/s, the maximum injection time was set to 50 ms and the dynamic exclusion time of tandem MS was 15 s to avoid repeated scanning of parent ions.

Database search

Maxquant (v1.5.2.8) was used to retrieve the secondary mass spectrometry data. Retrieval parameter setting: the database is Mus_musculus_10090 (17,045 sequences), reverse database is added to calculate the false discovery rate (FDR) caused by random matching, and common pollution database is added to the database to eliminate the influence of the contaminated protein in the identification results. The enzymatic cutting mode is set to trypsin/p and the number of missing bits is set to 2. The minimum length of peptide segment is set to 7 amino acid residues and the maximum modification number of peptide segment is set to 5. The mass error tolerance of first search and main search are 10 ppm and 5 ppm respectively, and the mass error tolerance of second fragment ion is 0.02 Da. The alkylation of cysteine was set as fixed modification, variable modification as Acetyl (Protein N-term), Oxidation (M), deamination (NQ) and Phospho (STY). The quantitative method was tmt-6plex, and the FDR of protein identification and PSM identification was set to 1%.

Bioinformatic analysis

Gene Ontology (GO), domain, the Kyoto Encyclopedia of Genes and Genomes (KEGG) annotation and subcellular localization were performed. GO annotation proteome was obtained from the UniProt-GOA database (<http://www.ebi.ac.uk/GOA/>) and completed with InterProScan. Identified proteins domain functional descriptions were annotated by InterProScan (<http://www.ebi.ac.uk/interpro/>). KEGG database was used to annotate pathways by KAAS and KEGG mapper. Subcellular location was predicted by using WoLF PSORT. Further hierarchical clustering of protein functional classification base on differential expression (such as GO, domain, pathway, complex). The database number or protein sequence of differential expression protein screened from different comparison groups were compared with the STRING (v.11.0) protein network interaction database, and the interaction relationship of differential protein was extracted if the confidence score >0.7 (high confidence). Then, R package "networkD3" tool was used to visualize the interaction network of different proteins.

QUANTIFICATION AND STATISTICAL ANALYSIS

The statistics used in the bioinformatic analysis are described in the [STAR method](#) section above. The exact number of animals in this study has been indicated in the section of "[Transduction and infection of mice](#)". Wilcox's test and Benjamini-Hochberg correction are used to calculate and adjust p value, respectively. The criterions for determining differential expression between H and E group in transcriptome, proteome and phosphoproteome are indicated in the figure legends.